Atmospheric Environment 244 (2021) 117939

Contents lists available at ScienceDirect

Atmospheric Environment

journal homepage: http://www.elsevier.com/locate/atmosenv

$PM_{2.5}$ chemistry, organosulfates, and secondary organic aerosol during the 2017 Lake Michigan Ozone Study

Dagen D. Hughes [a], Megan B. Christiansen [b], Alissa Milani [a], Michael P. Vermeuel [c], Gordon A. Novak [c], Hariprasad D. Alwe [d], Angela F. Dickens [e], R. Bradley Pierce [f], Dylan B. Millet [d], Timothy H. Bertram [c], Charles O. Stanier [b], Elizabeth A. Stone [a,b,*]

[a] Department of Chemistry, University of Iowa, Iowa City, IA, USA
[b] Department of Chemical and Biochemical Engineering, University of Iowa, Iowa City, IA, USA
[c] Department of Chemistry, University of Wisconsin, Madison, WI, USA
[d] Department of Soil, Water, and Climate, University of Minnesota, St. Paul, MN, USA
[e] Wisconsin Department of Natural Resources, Madison, WI, USA
[f] Space Science and Engineering Center, University of Wisconsin, Madison, WI, USA

HIGHLIGHTS

- $PM_{2.5}$ composition differed across three periods of elevated ozone.
- Isoprene-derived organosulfates contribute substantially to secondary organic aerosol (SOA).
- SOA tracers indicate transformations occurred via photooxidation and ozonolysis.
- SOA formation was highly sensitive to aerosol acidity and inorganic sulfate.

GRAPHICAL ABSTRACT

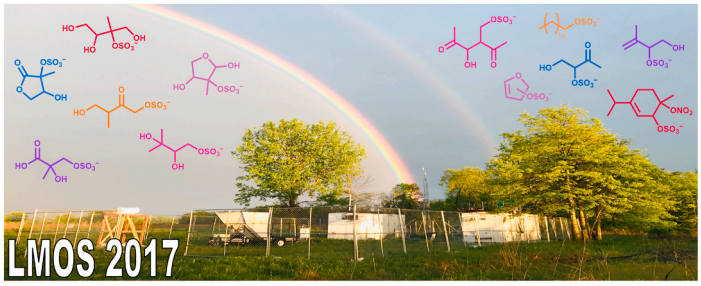

ARTICLE INFO

Keywords:
Atmospheric aerosols
Chemical composition
Isoprene
$PM_{2.5}$
Secondary organic aerosol
Organosulfates

ABSTRACT

The Lake Michigan Ozone Study from 21 May to 23 June 2017 (LMOS 2017) aimed to better understand the anthropogenic and biogenic sources that contribute to ozone and fine particles ($PM_{2.5}$) along the coast of Lake Michigan. Here, we focus on the chemical composition of daytime and nighttime $PM_{2.5}$—especially organic carbon, inorganic ions and organosulfates—at a ground-based supersite in Zion, Illinois. $PM_{2.5}$ mass concentrations ranged from 1.5 to 12.9 μg m^{-3} with an average (±standard error) of 5.2 ± 0.4 μg m^{-3}. The most significant contributor to $PM_{2.5}$ mass was organic matter (OM; calculated as 1.7 × organic carbon [OC]; contributing an average of 59 ± 2%), followed by sulfate (17 ± 1%), ammonium (6.3 ± 0.3%), nitrate (3.5 ± 0.4%), and elemental carbon (EC; 3.4 ± 0.2%). During each of the three periods of high ozone, $PM_{2.5}$ had different regional characteristics. Period A (2–3 June) was impacted by lake breeze and south-easterly air masses that travelled over major urban areas. Period A had the highest daily $PM_{2.5}$ mass concentrations (11.4 ± 1.5 μg m^{-3}) and EC with a relatively low OC:EC ratio of 7.0, indicating the influence of sources with low OC:EC ratios, which includes the anthropogenic combustion of fossil fuels and biomass. Period B (10–13 June) was impacted by air masses traveling from the southern US. It had a relatively high OC:EC ratio of 18, the highest $PM_{2.5}$ sulfate

* Corresponding author. Department of Chemistry, University of Iowa, Iowa City, IA, USA.
E-mail address: betsy-stone@uiowa.edu (E.A. Stone).

https://doi.org/10.1016/j.atmosenv.2020.117939
Received 20 May 2020; Received in revised form 11 September 2020; Accepted 15 September 2020
Available online 17 September 2020

concentrations and aerosol acidity, and elevated mixing ratios of isoprene along with its oxidation products methyl vinyl ketone (MVK) and methacrolein (MACR). Peak concentrations of organosulfates, including methyltetrol sulfate (m/z 215; $C_5H_{11}SO_7^-$), were also observed throughout period B. Period C (13–17 June) followed a change to northerly winds. $PM_{2.5}$ concentrations decreased along with decreases in sulfate, acidity, and most organosulfates. Throughout the study, organosulfates accounted for an average of 4% of OM and up to 15% of OM in Period B. Organosulfates were largely isoprene-derived, with lessor contributions from monoterpenes (0.3%) and anthropogenic sources (0.5%). Through these measurements of organosulfates in the Great Lakes region, we demonstrate the importance of anthropogenic sulfate emissions and aerosol acidity on SOA formation, and establish that isoprene-derived organosulfates, in particular, contribute significantly to $PM_{2.5}$. With other LMOS observations, the chemical signatures of $PM_{2.5}$, and back trajectories show that ozone episodes cooccur with localized lake-breeze meteorology within air masses that vary from episode to episode in chemical history and source region.

1. Introduction

Atmospheric fine particulate matter ($PM_{2.5}$; particles $\leq$ 2.5 μm in aerodynamic diameter) is a criteria air pollutant regulated by National Ambient Air Quality Standards (NAAQS). $PM_{2.5}$ includes inorganic and organic species of natural and anthropogenic origin that are emitted directly (primary) or formed in the atmosphere as secondary aerosol. The latter category includes secondary organic aerosol (SOA) derived from volatile organic compounds (VOCs) and secondary inorganic aerosol derived primarily from NH_3, SO_2, and NO_2. $PM_{2.5}$ adversely affects human health (Kampa and Castanas, 2008; Valavanidis et al., 2008) and influences Earth's climate through direct and indirect radiative forcing (Haywood and Boucher, 2000). These effects are influenced by the composition of $PM_{2.5}$ which is region-specific and variable due to differences in sources, meteorology, and geography (Atkinson, 2000; Lee and Hopke, 2006; Schlesinger, 2007; Whiteaker et al., 2002). The chemical composition of $PM_{2.5}$ can yield insight to its sources and chemical transformations in the atmosphere. Combined with receptor modelling, PM composition data can be used to estimate the absolute and relative impacts of PM sources in a specific region (Hopke, 2016; Singh et al., 2017).

A significant, albeit uncertain, fraction of $PM_{2.5}$ is SOA produced from biogenic and anthropogenic precursors (De Gouw et al., 2005; Hallquist et al., 2009; Kanakidou et al., 2005). Of the known SOA precursors, biogenic VOCs, such as isoprene (2-methyl-1,3-butadiene; C_5H_8) and monoterpenes ($C_{10}H_{16}$), are among the most significant contributors to SOA due to their large global emission rates and high reactivities with atmospheric oxidants. Isoprene is the most prevalent non-methane hydrocarbon emitted into the atmosphere with yearly emission rates exceeding 500 Tg (Guenther et al., 2012). The photooxidation of isoprene—primarily initiated by the hydroxyl radical (OH) along with contributions from ozone, nitrate radicals, and chlorine atoms—has been estimated to account for as much as 50% of the global SOA budget (Henze and Seinfeld, 2006; Zhang et al., 2007). Ozone can affect SOA formation, for example, by scavenging nitrogen oxides (NO_x) (Li et al., 2019; Meng et al., 1997) and form SOA via ozonolysis of isoprene and other VOCs (Carlton et al., 2009).

Organosulfates in $PM_{2.5}$ form by reactions of VOCs in the presence of acidic sulfate (Surratt et al., 2007, 2010) and are estimated to account for as much as 5–10% of the organic mass across the continental US (Tolocka and Turpin, 2012). They are primarily formed via the acid-catalyzed reactive uptake of gas-phase epoxides onto sulfate aerosol (Surratt et al., 2010), but have also been found to form by the nucleophilic substitution of organic nitrate by sulfate (Darer et al., 2011) and through the oxidation of VOCs via sulfate radical anions (Nozière et al., 2010; Schindelka et al., 2013). Through a combination of chamber experiments and field studies, organosulfates have been shown to form readily from biogenic precursors which include isoprene (Surratt et al., 2007), monoterpenes (Iinuma et al., 2009), sesquiterpenes (Chan et al., 2011), 2-methyl-3-buten-2-ol (MBO) (Zhang et al., 2012), and 3-Z-hexenal (Shalamzari et al., 2014). Because sulfate is primarily a product of fossil fuel combustion (Carlton et al., 2010), organosulfates can be used to trace biogenic SOA influenced by anthropogenic emissions.

The Lake Michigan Ozone Study 2017 (LMOS 2017) was a collaborative field campaign with the broad goal of better understanding air quality in the Lake Michigan region through airborne, ship, mobile, and ground-based measurements of meteorology, gas-phase chemistry, and $PM_{2.5}$ composition (Pierce et al., 2016). Coastal regions, like this one, experience ozone exceedances that can result from unique coastal meteorology in which urban pollution reacts in a shallow stable boundary layer over the water to form ozone that is advected back to shore by prevailing winds or by diurnal breezes off the lake (Dye et al., 1995; Hastie et al., 1999), sea (Angevine et al., 2004; Banta et al., 2011), or bay (Loughner et al., 2014). Our study of $PM_{2.5}$ helps to understand the complex, multiphase chemistry occurring during ozone exceedences. In addition, it provides new insights to $PM_{2.5}$ in the region.

Previous studies have characterized atmospheric PM in the Great Lakes region and found that a significant portion of $PM_{2.5}$ is secondary and predominantly composed of organic matter (OM), sulfate, nitrate, and ammonium (Bullard et al., 2017; Jeong et al., 2011; Kim et al., 2005; Sheesley et al., 2004). Sources of $PM_{2.5}$ in the Great Lakes region are commonly attributed to regional secondary aerosol (SOA, sulfate, and nitrate), mobile sources (gasoline-powered vehicles and diesel combustion), and local sources (i.e. industrial processes) (Buzcu-Guven et al., 2007; Morishita et al., 2011; Rizzo and Scheff, 2007; Stone et al., 2009). Single-particle measurements from a mixed forest in northern Michigan have demonstrated diel transitions in SOA composition and phase state, in which daytime particles were more impacted by isoprene-derived SOA and sulfate, while nighttime particles had a larger impact of terpene-derived SOA (Slade et al., 2019). Sulfate, nitrate, and oxalate concentrations in northern Chicago were lowest in air masses originating over the lake, and highest in air masses impacted by industrial activities to the south (Fosco and Schmeling, 2007). Other studies investigating the transport of atmospheric aerosols over Lake Michigan predict that lake-breeze circulations transport atmospheric particles originating in Chicago northward (Harris and Kotamarthi, 2005) and that anthropogenic SOA reaches a regional maximum alongside ozone over southern Lake Michigan (Spak and Holloway, 2009).

Our study has two primary objectives. First, we evaluate how $PM_{2.5}$ concentrations and composition in Zion, Illinois vary across three distinct periods of elevated ozone during LMOS 2017. Second, we identify the major organosulfates, quantify/semi-quantify their contribution to $PM_{2.5}$, and assess differences in SOA formation between periods of elevated ozone compared to background periods. The detailed chemical speciation of atmospheric $PM_{2.5}$ is intended for use in future source apportionment modelling and chemical transport model evaluation. Additionally, this work delivers one of the first measurements of organosulfates in the upper Midwestern US and provides new insights into the relationship between ozone and $PM_{2.5}$ composition.

2. Materials and methods

2.1. Chemicals and reagents

Authentic standards utilized for instrument calibration include a six-cation and seven-anion solution (Dionex), methyl sulfate (Sigma Aldrich), and ethyl sulfate (Sigma Aldrich). Standards for glycolic acid sulfate, hydroxyacetone sulfate, and acetoin sulfate were synthesized (potassium salts, >95% purity) as described in Hettiyadura et al. (2015). Ultra-pure water was generated on site (Thermo, Barnsted EasyPure-II; 18.2 MΩ cm resistivity, OC < 40 μg L^{-1}). Acetonitrile (Optima, Fisher Scientific), ammonium acetate (≥99%, Sigma Aldrich), and ammonium hydroxide (Optima, Fisher Scientific) were used as received.

2.2. $PM_{2.5}$ sample collection

Ground-based measurements for LMOS 2017 were conducted at an Illinois Environmental Protection Agency (EPA) monitoring site in Zion, Illinois (42.468°N, 87.810°W; city population: 23 705) located within the Illinois Beach State Park just south of the Wisconsin border, 0.95 km inland from the shoreline of Lake Michigan, and 65 km north of Chicago, Illinois (population: 2.7 million). The site was surrounded by dunes, marshes, prairies, and forests with no major point sources between sample collection location and the lakeshore. $PM_{2.5}$ was collected using two medium volume air samplers (3000B, URG Corporation) equipped with a cyclone operating at a flow rate of 90 L min^{-1}. One sampler collected $PM_{2.5}$ on prebaked (550 °C for 18 h) 90 mm quartz fiber filters (QFFs; Pallflex Tissuequartz, Pall Life Sciences). The second sampler collected $PM_{2.5}$ using a dual-stage filter holder. The first stage collected particulate matter on 47 mm Teflon filters (PTFE Membrane, Pall Life Sciences), while the second stage, used to account for organic gas adsorption during sampling, utilized prebaked (550 °C for 18 h) 47 mm QFFs (Pallflex Tissuequartz, Pall Life Sciences). $PM_{2.5}$ samples were collected twice daily from 08:00 to 20:00 CDT (daytime) and from 20:30 to 07:30 CDT (nighttime) the following day. The 12-h sampling period for daytime samples was selected following the analysis of historical meteorological data at Zion during which the onset of lake breeze circulations was observed as early as 08:00 and as late as 18:00. Field blanks were collected every five samples following the same sampling procedure without passing air through the sampler. Following collection, QFFs were stored in aluminium foil (prebaked at 550 °C for 5.5 h) lined Petri dishes whereas the Teflon filters were stored in unlined Petri dishes. The Petri dishes were sealed with Teflon tape and stored at −20 °C until analysis.

2.3. Measurements of mass, organic carbon, and elemental carbon

$PM_{2.5}$ mass was determined gravimetrically using a high-precision balance (XP26, Mettler-Toledo). The 47 mm Teflon filters were weighed pre- and post-sampling in a humidity (<40% RH) and temperature-controlled (22–25 °C) chamber. Elemental carbon (EC) and organic carbon (OC) were measured by thermal-optical analysis (Sunset Laboratory) following the Aerosol Characterization Experiment (ACE)-Asia base case protocol described by Schauer et al. (2003). Organic carbon was corrected for gas adsorption artifacts by subtracting OC measured on 16 backup QFFs collected after Teflon filters in the dual-stage filter holder. The magnitude of the artefact averaged 0.3% for daytime samples and 0.2% for nighttime samples.

2.4. Water-soluble ion analysis

Water-soluble cations and anions were extracted using a procedure adapted from Jayarathne et al. (2014). Briefly, Teflon filters were cut in half using a ceramic blade on a clean glass surface. Mass measurements of the filter were taken before and after filter cutting using an analytical balance (Mettler Toledo XS204) to determine the fraction of filter extracted. One-half of the filter was extracted with 4.00 mL of ultra-pure water by shaking (10 min), sonicating (30 min), and then shaking (10 min). The extracts were filtered with a polypropylene membrane syringe filter (0.45 μm pore size; Puradisc, Whatman) and quantified using ion exchange chromatography (Dionex IonPac CS12A cation column and Dionex IonPac AS22 anion column) with suppressed conductivity detection (ICS5000, Dionex).

2.5. Organosulfate analysis

2.5.1. Extraction of organosulfates

Organosulfates were extracted following the method described in Hettiyadura et al. (2015). Briefly, sub-samples of the QFFs were extracted via sonication in 10 mL acetonitrile and ultra-pure water (95:5, v/v) for 20 min. The extracts were filtered through a polypropylene membrane syringe filter (0.45 μm pore size; Puradisc, Whatman), evaporated to dryness under ultra-high purity nitrogen at 50 °C (Turbovap LV, Caliper Life Sciences; Reacti-Vap I 18825, Thermo Scientific), and reconstituted to a final volume of 100 μL using 95:5 (v/v) acetonitrile: ultra-pure water. Extraction recoveries were determined as the ratio of organosulfate recovered from the extraction to the organosulfate spiked onto a filter. Efficient recoveries were obtained for a range of compounds: methyl sulfate (85–115%), ethyl sulfate (83–123%), hydroxyacetone sulfate (86–114%), acetoin sulfate (81–112%), and glycolic acid sulfate (78–116%).

2.5.2. Quantitation of organosulfates

Using the optimized conditions described in Hettiyadura et al. (2017), an ultra-performance liquid chromatograph (UPLC) interfaced to a triple quadrupole mass spectrometer with negative electrospray ionization ((−)ESI-TQD) operating in multiple reaction monitoring (MRM) mode was utilized for quantifying five organosulfates. The dynamic linear range for each compound was between 0.5 and 500 μg L^{-1} with coefficient of determination (R^2) greater than 0.995 and detection limits reported in Hettiyadura et al. (2015). Separation was achieved using hydrophilic interaction liquid chromatography (HILIC) on an ethylene bridged hybrid amide (BEH-amide) column (2.1 × 100 mm, 1.7 μm particle size; AQCUITY UPLC Waters). The eluents, delivered as a gradient outlined by Hettiyadura et al. (2015), included an organic eluent of ammonium acetate buffer (10 mM, pH 9) in acetonitrile and ultra-pure water (95:5, v/v) and an aqueous eluent of ammonium acetate buffer (10 mM, pH 9) in ultra-pure water. Data was acquired and analyzed using MassLynx and QuanLynx software (Waters Inc., Version 4.1).

2.5.3. Semi-quantification and identification of organosulfates

Due to the limited availability of authentic standards, additional organosulfate species were semi-quantified using surrogate standards. In MRM, the TQD detects specific precursor-to-fragment transitions. For organosulfates, the fragment ion was either the bisulfate anion (*m/z* 97) or the sulfate radical anion (*m/z* 96), and the precursor ions ($[M\text{-}H^+]^-$) were identified using HILIC-TQD in precursor ion mode scanning masses ranging from 100 to 400 Da. Organosulfates were further characterized by (−) ESI time-of-flight mass spectrometry (TOF-MS) (Bruker Daltonics MicrOTOF) following HILIC to determine their monoisotopic mass and elemental composition. Data was acquired and analyzed using MassLynx and Quanlynx software (Waters Inc., Version 4.1) and molecular formulas were assigned considering both odd and even electron states, $C_{0\text{-}20}$, $H_{0\text{-}50}$, $N_{0\text{-}10}$, $O_{0\text{-}10}$, $S_{0\text{-}6}$, and a maximum error of 5 mDa. Hydroxyacetone sulfate, glycolic acid sulfate, and methyl sulfate were utilized as surrogate standards to semi-quantify the organosulfates eluting before four minutes in the precursor to *m/z* 97 scan, eluting after four minutes in the precursor to *m/z* 97 scan, and eluting before four minutes in the precursor to *m/z* 96 scan, respectively.

2.6. Analysis of 2-methyltetrols, 2-methylglyceric acid, and levoglucosan

Isoprene SOA tracers 2-methylthreitol and 2-methylerythritol (collectively known as 2-methyltetrols) along with 2-methylglyceric acid and levoglucosan were measured by gas chromatography mass spectrometry (GC-MS) as described by Al-Naiema and Stone (2017). Briefly, sub-samples of each filter were spiked with isotopically labelled succinic acid as an internal standard for 2-methyltetrols and 2-methylglyceric acid along with levoglucosan-$^{13}C_6$ for levoglucosan. The sub-samples were extracted sequentially with three 10 mL portions of acetonitrile for 15 min by ultrasonication. The combined extracts were reduced to 2 mL via rotary evaporation at 30 °C, 120 rpm, and 200 mbar. Extracts were filtered with 0.25 PTFE syringe filters (Whatman) and stored frozen at −20 °C until analysis. Immediately prior to analysis, the extracts were evaporated to 50 μL under ultra-high purity nitrogen at 30 °C. A 20 μL aliquot of the extract was evaporated to dryness under a gentle stream of ultra-high purity nitrogen at 30 °C and trimethylsilyated with 10 μL of N,O-bis(trimethylsilyl)trifluoroacetamide and trimethylchlorosilane (BSTFA + TMCS, 99:1, Fluka Analytical 99%). The mixture was reacted at 100 °C for 90 min and then analyzed by GC-MS.

2.7. Collocated measurements

LMOS 2017 featured a suite of meteorological, gas-phase, and aerosol measurements. These included isoprene, methyl vinyl ketone (MVK), and methacrolein (MACR) along with an ensemble of other VOCs obtained by proton transfer reaction quadrupole interface time-of-flight mass spectrometry (PTR-QiTOF, Ionicon Analytik, GmbH) as described in Millet et al. (2018). Measurements of nitric acid were obtained using a chemical ionization time-of-flight mass spectrometer (Tofwerk AG, Switzerland, and Aerodyne Research Inc., USA) as described by Bertram et al. (2011). These measurements in LMOS 2017 are discussed in further detail by Vermeuel et al. (2019) and were averaged here to one hour for comparison to PM. Onsite measurements of ozone, NO_x, and meteorological conditions were provided by the Illinois EPA via the EPA's Air Quality System database.

2.8. Data analysis

Pearson's correlation coefficients were assessed using Minitab software. Correlations were classified as very strong (r = 0.9–1.0), strong (0.7–0.9), moderate (0.5–0.7), weak (0.3–0.5), or negligible (0.0–0.3). The correlations were tested at the 95% confidence interval such that correlations with p-values less than 0.05 were considered statistically significant.

Aerosol acidity was calculated using the thermodynamic equilibrium model ISORROPIA II (version 2.3) to predict the equilibrium portioning of species between the gas and particle phase. Model inputs included aerosol and gas phase species (NO_3^- + HNO_3, NH_4^+ + NH_3, SO_4^{2-}, Na^+, K^+, Ca^{2+}, and Mg^{2+}), temperature, and relative humidity. Notably, the ISORROPIA II model only considers the contribution of inorganic species and neglects the contribution of organic acids which has been shown to influence aerosol acidity at specific locations (Jin et al., 2020). Due to the low vapor pressure of sulfuric acid, $PM_{2.5}$ sulfate was assumed to represent total sulfate. Additionally, given the low atmospheric abundance (<0.05 μg m^{-3}) of chloride, this species was neglected. Gas phase ammonia was simulated using the Weather Research and Forecasting with Chemistry (WRF-Chem) model described in Abdi-Oskouei et al. (2020) as field measurements were not available. ISORROPIA II was run in the forward mode and thermodynamically stable phase state. Sensitivity tests to modelled ammonia concentrations were conducted and are depicted in Fig. S1.

Air trajectories were calculated using the Hybrid Single-Particle Lagrangian Integrated Trajectory (HYSPLIT) model system developed by the National Oceanic and Atmospheric Administration's Air Resources Laboratory (Rolph et al., 2017; Stein et al., 2015). HYSPLIT was ran online via the Real-time Environmental Applications and Display sYstem (READY) using meteorological data from the High-Resolution Rapid Refresh (version 1) with 3 × 3 km spatial resolution and 1 h temporal resolution. For each of the 65 filter samples, 48 h backward trajectories were initialized every hour (yielding 780 total trajectories) at 50 m above ground level.

3. Results and discussion

3.1. Ozone concentrations, meteorology, and relationship to $PM_{2.5}$ during LMOS 2017

$PM_{2.5}$ mass and ozone generally trended together (Fig. 1). Hourly ozone concentrations were fairly low from 22 May – 1 June, with daily maxima <60 ppbv (Fig. 1b). Lake breeze meteorology and elevated hourly ozone concentrations (>70 ppbv) were observed on 2 June and numerous times throughout 10–12 June and 14–16 June, hereafter referred to as ozone periods A, B, and C, respectively. Days are designated as "non-ozone events" when hourly ozone concentrations did not exceed 70 ppbv. Periods with elevated ozone exhibited "lake-breeze" meteorology to varying extents (Fig. S2). Ozone period A (08:00 on 2 June – 07:30 on 3 June) had the highest hourly ozone concentration (91 ppbv at 15:00–16:00) and PM levels. The meteorology at this time exhibited lake breeze characteristics with south-westerly winds observed at Zion in the early morning followed by a dramatic shift to onshore, south-easterly winds between 09:00 and 10:00 (Fig. S3). The lake breeze was deep (penetrating 5 km inland) and was maintained for 10 h during which time urban plumes originating in Gary, Indiana and Chicago, Illinois were transported to Zion after being processed over southern Lake Michigan (Abdi-Oskouei et al., 2020; Vermeuel et al., 2019). Ozone period B (08:00 on 10 June – 07:30 on 13 June) primarily had south-westerly winds with shallow lake breezes (penetrating 1 km inland) observed on 11 and 12 June (Fig. S4). Ozone concentrations during period B peaked at 76 ppbv between 11:00–12:00 on 12 June. $PM_{2.5}$ mass decreased between ozone period B (average ± standard error; 8.3 ± 1.4 μg m^{-3}) and ozone period C (08:00 on 14 June – 07:30 on 17 June; 5.7 ± 0.3 μg m^{-3}), concurrent with a decrease in average temperature (26.3 °C to 22.8 °C) and an increase in relative humidity (53% to 75%) (Fig. S2). Ozone period C had more variable winds ranging from easterly to south-westerly (Fig. S5). A deep lake breeze was observed briefly on 14 June whereas shallow lake breezes were observed throughout the afternoon on 15 and 16 June. Ozone concentrations during period C peaked at 88 ppbv between 14:00–15:00 on 15 June. Though lake breeze meteorology was common across the three ozone periods, air masses for each time period came from different regions.

3.2. Average $PM_{2.5}$ composition

The ambient concentrations of $PM_{2.5}$ mass, OM (calculated as 1.7 × OC), EC, and water-soluble inorganic ions for each sample are shown in Fig. 1a, with ranges and mean concentrations summarized in Table 1. Throughout the study, the largest contributor to $PM_{2.5}$ mass was OM (59%) while OC:EC averaged 12. During period A (Fig. 2a), the EC and OC concentrations peaked and exhibited lower OC:EC (7.0) than periods B (18), C (11) and non-ozone episodes (12). In comparison to summertime studies using similar methodology, the relatively high OC:EC ratio in Zion was similar to those observed in Iowa City, Iowa (11.1; Hughes and Stone, 2019) and Seney, Michigan (9.0; Sheesley et al., 2004) and much higher than the ratio observed in Chicago, Illinois (3.1; Morishita et al., 2011). The former areas have been shown to have a large influence from summertime SOA formation, suggesting that the enhancement of this ratio in Zion is due to contributions from non-combustion sources of OC, likely SOA (Cabada et al., 2004; Lim et al., 2003), while the lower ratio for period A suggests that PM had a greater influence from primary combustion sources. Biomass burning was ruled out as a major source of $PM_{2.5}$ based on low concentrations of gas-phase tracers

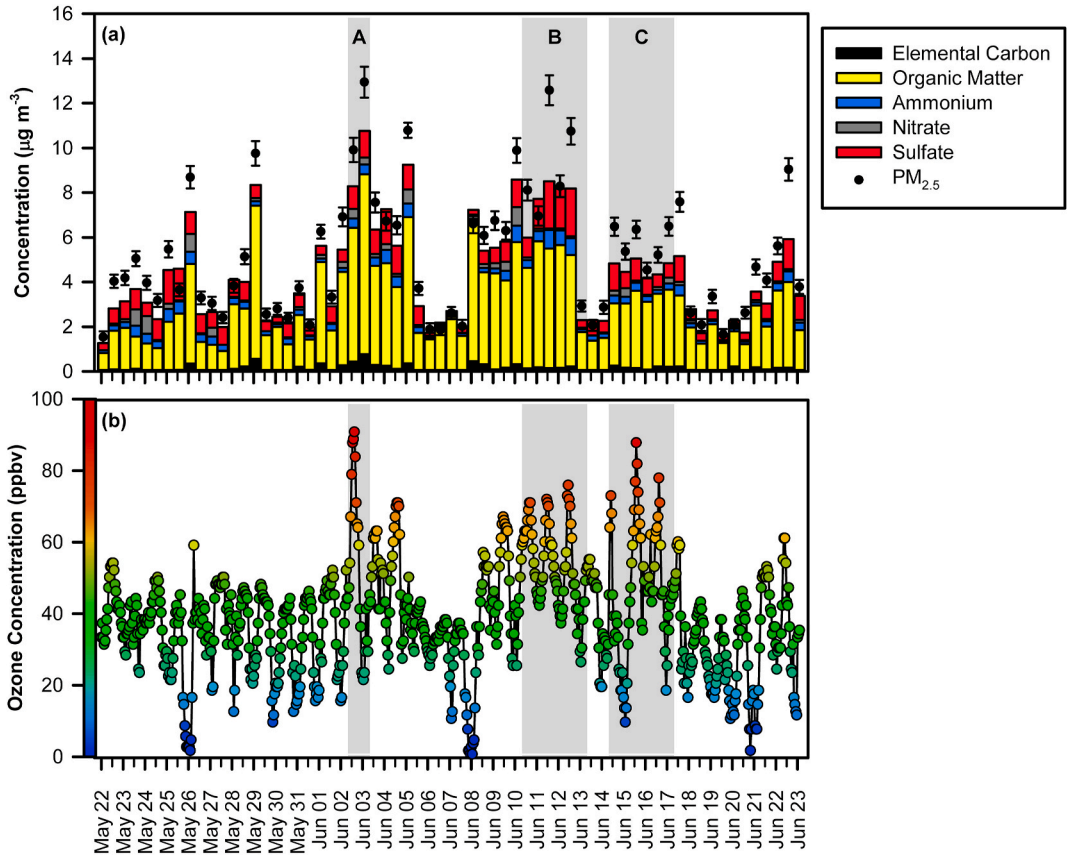

Fig. 1. Concentrations of (a) $PM_{2.5}$ mass, elemental carbon, organic matter (calculated as 1.7 × OC), ammonium, nitrate, and sulfate relative to (b) hourly ozone concentrations measured throughout the study period. The error bars represent the standard deviation and dates are defined using local time (CDT).

Table 1
Average concentrations (μg m^{-3}) of $PM_{2.5}$ mass, elemental carbon (EC), organic carbon (OC), organic matter (OM), and inorganic ions measured throughout the LMOS 2017 campaign (n = 65) and during ozone period A (n = 2), ozone period B (n = 6), ozone period C (n = 6), and non-ozone episodes (samples during which hourly ozone did not exceed 70 ppbv; n = 49). Standard error is given in parenthesis.

Component	LMOS 2017 Campaign 21 May 08:30–23 June 07:30			Ozone Period A 2 June 08:00 – 3 June 07:30		Ozone Period B 10 June 08:00 – 13 June 07:30		Ozone Period C 14 June 08:00 – 17 June 07:30		Non-Ozone Episodes	
	Range	Average	%PM	Average	%PM	Average	%PM	Average	%PM	Average	%PM
$PM_{2.5}$	1.5–12.9	5.2 (0.4)		11.4 (1.5)		8.3 (1.3)		5.7 (0.3)		4.2 (0.3)	
EC	<0.05–0.78	0.22 (0.02)	3.4	0.6 (0.2)	5.3	0.17 (0.01)	2.0	0.19 (0.03)	3.2	0.20 (0.02)	3.7
OC	0.49–4.7	1.8 (0.1)	35	4.1 (0.6)	36	2.7 (0.4)	35	1.9 ()	3	1.5 (0.1)	35
OM (1.7 × OC)	0.83–8.0	3.0 (0.2)	59	7.0 (1.0)	61	4.6 (0.6)	59	3.1 (0.1)	56	2.5 (0.2)	59
Sulfate	<0.02–3.1	0.8 (0.1)	17	1.1 (0.1)	9.7	1.4 (0.3)	17	0.8 (0.1)	14	0.7 (0.1)	17
Nitrate	<0.02–0.80	0.19 (0.03)	3.5	0.37 (0.06)	3.4	0.09 (0.01)	1.3	0.19 (0.05)	3.3	0.19 (0.03)	3.8
Ammonium	<0.002–0.83	0.31 (0.02)	6.3	0.43 (0.01)	3.8	0.5 (0.1)	6.1	0.29 (0.03)	5.0	0.27 (0.02)	6.6
Sodium	<0.009–0.12	0.043 (0.004)	0.7	0.04 (0.01)	0.4	0.06 (0.02)	0.7	0.041 (0.004)	0.7	0.043 (0.005)	0.8
Potassium	<0.004–0.10	0.029 (0.003)	0.6	0.06 (0.02)	0.5	0.04 (0.01)	0.6	0.029 (0.002)	0.5	0.026 (0.003)	0.6
Magnesium	<0.001–0.05	0.012 (0.001)	0.2	0.04 (0.01)	0.4	0.021 (0.004)	0.3	0.017 (0.005)	0.3	0.009 (0.001)	0.2
Calcium	<0.008–0.19	0.06 (0.01)	1.1	0.12 (0.03)	1.1	0.10 (0.02)	1.3	0.06 (0.02)	1.0	0.05 (0.01)	1.1

(Vermeuel et al., 2019) and levoglucosan, a tracer for biomass burning PM (Fig. S7).

The presence of secondary aerosol was also indicated by contributions from sulfate (17%), ammonium (6%), and nitrate (4%) derived via conversion of their gaseous precursors SO_2, NO_x, and NH_3, respectively (Allen and Turner, 2008). Ammonium correlated very strongly with sulfate (r = 0.939, p-value < 0.001) reflecting their co-occurrence as ammonium sulfate salts. Nitrate correlated weakly with ammonium (r = 0.403, p-value = 0.002) which is likely explained by the reversible reaction of ammonium nitrate and its dependence on temperature (Spicer, 1977; Stelson and Seinfeld, 1982). A weak negative correlation between nitrate and temperature (r = −0.303, p-value = 0.025) is consistent with increasing temperatures shifting the partitioning of nitrate from the particle to the gas phase as nitric acid (Aw and Kleeman, 2003). In total, the measured components accounted for 91% of $PM_{2.5}$ mass on average, which is comparable to prior studies in the Midwestern US (Buzcu-Guven et al., 2007; Jayarathne et al., 2016; Morishita et al., 2011; Pancras et al., 2013).

3.3. Organosulfates during LMOS 2017

3.3.1. Quantitative analysis

The ambient concentrations of the organosulfates quantified using authentic standards are shown in Table 2. The two most abundant

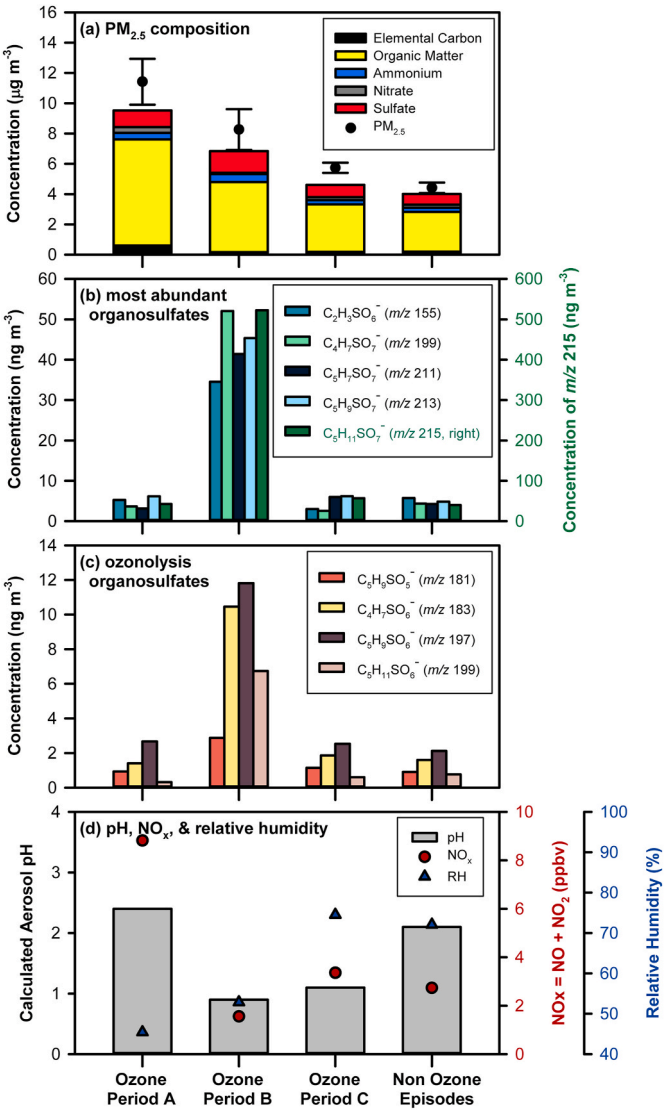

Fig. 2. Concentrations of (a) bulk $PM_{2.5}$ components, (b) five abundant organosulfates, and (c) four organosulfates uniquely formed via isoprene ozonolysis relative to (d) aerosol pH, NO_x concentration, and relative humidity throughout ozone period A (2 June), ozone period B (10–12 June), ozone period C (14–16 June), and non-ozone episodes. The error bars represent the standard error.

organosulfates quantified were hydroxyacetone sulfate (Fig. 3a) and glycolic acid sulfate (Fig. 3b). Both species correlated strongly with sulfate ($r = 0.773$ and 0.768; p-values < 0.001), reflecting the key role sulfate plays in organosulfate formation as a reactant and source of aerosol acidity. Similar relationships have been observed in the Southeastern US (Budisulistiorini et al., 2015; Hettiyadura et al., 2017; Rattanavaraha et al., 2016) and highlight the ability of anthropogenic pollutants to enhance isoprene-derived SOA. In the presence of acidic sulfate, hydroxyacetone sulfate has been reported to form via isoprene photooxidation (Surratt et al., 2008) and isoprene ozonolysis (Riva et al., 2016). Glycolic acid sulfate has been shown to form from glyoxal and more efficiently from glycolic acid (Liao et al., 2015). While glyoxal and glycolic acid have both anthropogenic and biogenic sources, glycolic acid sulfate has been primarily associated with isoprene oxidation (Liao et al., 2015). When compared to other summertime studies, the observed glycolic acid sulfate concentrations were a factor of two lower than those reported in Iowa City, Iowa (Hughes and Stone, 2019) and Centreville, Alabama (Hettiyadura et al., 2017), a factor of three lower than Birmingham, Alabama (Rattanavaraha et al., 2016), and similar to those in Bakersfield, California (Olson et al., 2011). Concentrations of hydroxyacetone sulfate were three times lower than those reported in Iowa City (Hughes and Stone, 2019) and four times lower than Centreville (Hettiyadura et al., 2017). Although the absolute concentrations of glycolic acid sulfate and hydroxyacetone sulfate were lower in Zion, they accounted for a greater fraction of total OC in Zion (0.51%) than in Iowa City (0.24%) and Centreville (0.15%) indicating a stronger relative influence on $PM_{2.5}$ from biogenic SOA. The five organosulfates quantified using authentic standards collectively accounted for 0.2% of $PM_{2.5}$ mass and 0.3% of OM in Zion. With previous estimates suggesting that organosulfates account for 6.7–8.4% of OM in the Midwestern US (Tolocka and Turpin, 2012), additional organosulfur species were identified and semi-quantified using surrogate standards.

3.3.2. *Semi-quantitative analysis of organosulfates*

Other organosulfates in $PM_{2.5}$ were screened by tandem mass spectrometry (MS/MS) following HILIC separation. The triple-quadrupole MS/MS operated in precursor ion mode, in which the instrument determines the precursors of relatively abundant sulfur-containing organosulfate fragment ions: the bisulfate anion (HSO_4^- at m/z 97) and the sulfate radical anion ($SO_4^{\bullet-}$ at m/z 96) (Attygalle et al., 2001). Our analysis focuses on precursors to m/z 96 and m/z 97, which are characteristic of organosulfates (Gómez-González et al., 2008; Iinuma et al., 2007b; Surratt et al., 2008). Precursors to the bisulfite anion (m/z 81) and sulfite radical anion (m/z 80) were not examined because they are largely redundant (Hettiyadura et al., 2017, 2019; Hughes and Stone, 2019).

Six day/night samples from the start (29–30 May), middle (6–7 June), and end (20–21 June) of the LMOS 2017 campaign were used for initial organosulfate identification by high-resolution TOF-MS. The organosulfate species identified were then semi-quantified in all LMOS samples. Utilizing surrogate standards for quantification does not account for differences in ionization efficiency and fragmentation patterns which may introduce positive or negative biases (Hettiyadura et al., 2017). The following discussion focuses on the observed organosulfate species that either: (1) exhibited relative intensity $\geq 1\%$ of the precursor ion signal; (2) are a unique product of isoprene ozonolysis (Riva et al., 2016); or (3) eluted after four minutes, when ionization is suppressed due to the mobile phase gradient shifting from acetonitrile to aqueous (Hettiyadura et al., 2017) but atmospheric abundance may be high. These selection criteria were utilized to focus our attention on organosulfates of high atmospheric abundance and maximize instrument sensitivity by limiting the number of ions monitored.

Ten organosulfates in the precursor to m/z 97 scan and two organosulfates in the precursor to m/z 96 scan met these selection criteria (Fig. 4). Together, these twelve organosulfates accounted for 63% of the m/z 97 precursor ion scan signal and 32% of the m/z 96 precursor ion scan signal. Stronger signals were observed in the precursor to m/z 97 scan, relative to the m/z 96 scan, due to the greater stability of the bisulfate anion compared to the sulfate radical anion. The semi-quantified organosulfate species observed in Zion are summarized in Table 3 along with their calculated monoisotopic mass, molecular formula determined using HILIC-TOF, molecular structures and expected precursor(s) based on previous chamber experiments and fieldwork, retention time, and relative contribution to their respective precursor ion signal.

The majority of the semi-quantified organosulfates were isoprene-related (8 out of 12 total) and accounted for 3.2 ± 0.4% OM on average (±standard error), indicating that $PM_{2.5}$ was heavily influenced by isoprene SOA. The most abundant organosulfate, methyltetrol sulfate ($C_5H_{11}SO_7^-$; m/z 215; Fig. 3d), is produced from the acid catalyzed nucleophilic addition of sulfate to isoprene epoxydiols (IEPOX) (Surratt et al., 2010). Four isomers of methyltetrol sulfate were baseline resolved and corresponded to secondary (retention time (t_R) of 1.30 and 1.58) and tertiary (t_R of 2.45 and 3.03) diastereomers (Cui et al., 2018). The four isomers detected in Zion are consistent with those in Iowa City,

Table 2
Average concentrations (ng m^{-3}) of organosulfates measured throughout the LMOS 2017 campaign and during ozone period A (n = 2), ozone period B (n = 6), ozone period C (n = 6), and non-ozone episodes (samples during which hourly ozone did not exceed 70 ppbv; n = 49).

Organosulfate	LMOS 2017 Campaign 21 May 20:30–23 June 7:30			Ozone Period A 2 June 08:00 – 3 June 07:30		Ozone Period B 10 June 08:00 – 13 June 07:30		Ozone Period C 14 June 08:00 – 17 June 07:30		Non-Ozone Episodes	
	Range	Average	%OM	Average	%OM	Average	%OM	Average	%OM	Average	%OM
$CH_3SO_4^-$ (*m/z* 111)[a] methyl sulfate	<0.03–0.71	0.23	0.01	0.29	0.004	0.39	0.1	0.27	0.01	0.20	0.01
$C_2H_5SO_4^-$ (*m/z* 125)[a] ethyl sulfate	<0.03–0.15	0.06	0.002	0.04	0.001	0.07	0.001	0.04	0.001	0.06	0.002
$C_3H_5SO_5^-$ (*m/z* 153)[b] hydroxyacetone sulfate	<0.03–10.97	1.63	0.1	1.03	0.02	6.29	0.1	1.67	0.1	1.04	0.04
$C_2H_3SO_6^-$ (*m/z* 155)[b] glycolic acid sulfate	<0.02–68.97	8.17	0.3	5.27	0.1	34.54	0.7	3.02	0.1	5.37	0.2
$C_4H_7SO_5^-$ (*m/z* 167)[b] acetoin sulfate	<0.07–0.71	0.13	0.003	0.09	0.001	0.18	0.003	0.10	0.003	0.12	0.004
$C_4H_5SO_5^-$ (*m/z* 165)[c]	<0.03–2.1	0.5	0.02	0.8	0.01	1.3	0.03	0.4	0.01	0.4	0.02
$C_5H_9SO_5^-$ (*m/z* 181)[d]	<0.03–5.5	1.1	0.04	0.9	0.01	2.9	0.06	1.2	0.04	0.9	0.04
$C_4H_7SO_6^-$ (*m/z* 183)[d]	<0.03–17.7	2.4	0.1	1.4	0.02	10.5	0.2	1.9	0.1	1.6	0.1
$C_5H_9SO_6^-$ (*m/z* 197)[d]	<0.03–18.4	3.1	0.1	2.7	0.04	11.8	0.2	2.5	0.1	2.0	0.1
$C_5H_{11}SO_6^-$ (*m/z* 199)[d]	<0.03–14.9	1.3	0.04	0.3	0.005	6.7	0.1	0.6	0.02	0.7	0.03
$C_4H_7SO_7^-$ (*m/z* 199)[e] methylglyceric acid sulfate	<0.02–84.2	8.8	0.2	3.7	0.1	52.1	1.0	2.6	0.1	4.0	0.1
$C_5H_7SO_7^-$ (*m/z* 211)[d]	<0.03–75.3	7.9	0.2	3.1	0.04	41.4	0.8	6.0	0.2	4.0	0.2
$C_5H_9SO_7^-$ (*m/z* 213)[d]	<0.03–76.3	8.9	0.2	6.2	0.1	45.4	0.9	6.2	0.2	4.6	0.2
$C_5H_{11}SO_7^-$ (*m/z* 215)[d] methyltetrol sulfate	<0.03–833	87.0	2.2	42.7	0.6	523	10.1	56.8	1.9	38.3	1.4
$C_7H_{11}SO_7^-$ (*m/z* 239)[d]	<0.03–21.1	3.6	0.5	2.5	0.2	10.5	0.3	2.7	0.1	2.8	0.1
$C_{12}H_{25}SO_4^-$ (*m/z* 265)[d]	<0.03–95.5	14.4	0.5	15.1	0.2	10.3	0.3	1.5	0.1	12.4	0.6
$C_{10}H_{16}NSO_7^-$ (*m/z* 294)[c]	<0.03–36.6	5.1	0.2	11.8	0.2	9.2	0.2	2.8	0.1	4.6	0.2

[a] Quantified using commercial standard.
[b] Quantified using synthesized standards.
[c] Quantified using methyl sulfate as a surrogate standard.
[d] Quantified using hydroxyacetone sulfate as a surrogate standard.
[e] Quantified using glycolic acid sulfate as a surrogate standard.

Iowa (Hughes and Stone, 2019), but do not include the primary diastereomers previously reported in Centreville, Alabama (Hettiyadura et al., 2017) and Atlanta, Georgia (Hettiyadura et al., 2019). The absence of these isomers in Zion and Iowa City suggests that the primary isomers of methyltetrol sulfate are less chemically stable (e.g. undergo hydrolysis) compared to the secondary and tertiary isomers (Cui et al., 2018; Darer et al., 2011). The organosulfates with the next highest signals were sulfate esters of cyclic methyltrihydroxyaldehyde hemiacetal ($C_5H_9SO_7^-$; *m/z* 213) and sulfate esters of methydihydroxylactone ($C_5H_7SO_7^-$; *m/z* 211), which have been observed during the photooxidation of isoprene (Surratt et al., 2008) and may be produced from the further oxidation of methyltetrol sulfate (Hettiyadura et al., 2015). 2-Methylglyceric acid sulfate ($C_4H_7SO_7^-$; *m/z* 199; Fig. 3f) was observed at a comparable concentration, and forms from isoprene oxidation products in the presence of sulfate under high NO_x conditions (Nguyen et al., 2015). Four organosulfates (*m/z* 181, 183, 197, and 199) uniquely formed from isoprene ozonolysis (Riva et al., 2016) were observed at lower concentrations (<5 ng m^{-3}) and highlight the direct influence of ozone on $PM_{2.5}$ composition (Fig. 2c). These four organosulfates were consistently detected throughout LMOS 2017 and accounted for 0.30 ± 0.01% OM on average. In general, the organosulfates from isoprene ozonolysis followed the same trend as the major organosulfates resulting from isoprene photooxidation with concentrations highest during ozone period B. Methyltetrol sulfate has also been shown to form from isoprene ozonolysis in addition to isoprene photooxidation (Riva et al., 2016) and is expected to form through a combination of photooxidation and ozonolysis pathways in Zion (Fig. 2b).

In addition to isoprene, organosulfate formation was also found to be influenced by monoterpenes (accounting for 2 of the 12 semi-quantified species) and anthropogenic sources (2 of 12). Monoterpene-derived organosulfates included an organosulfur species with the formula $C_7H_{11}SO_7^-$ (*m/z* 239) derived from the oxidation of limonene (Surratt et al., 2008) and a nitro-oxy organosulfate ($C_{10}H_{16}NSO_7^-$; *m/z* 294) formed from the oxidation of numerous monoterpenes in the presence of NO_x (Surratt et al., 2008). Organosulfates influenced by anthropogenic sources included $C_4H_5SO_5^-$ (*m/z* 165), which has been found to result from the photooxidation of cyclohexene (Liu et al., 2017), and dodecyl sulfate ($C_{12}H_{25}SO_4^-$; *m/z* 265), a common surfactant in detergents and wastewater treatment (Hettiyadura et al., 2017). Dodecyl sulfate was measured intermittently (58% of samples) but had the second-highest estimated concentration. This value is likely biased high because surfactants like dodecyl sulfate ionize efficiently under negative electrospray conditions (Cortés-Francisco and Caixach, 2013) and the utilized surrogate standard did not represent this. Together the observed organosulfates emphasize the influence of biogenic emissions—particularly isoprene—on SOA formation.

3.4. Factors influencing the composition and abundance of isoprene SOA in LMOS 2017

The average concentrations of organosulfates and their contribution to aerosol OM during ozone periods A–C and non-ozone episodes are summarized in Table 2. While similar organosulfur species were observed during the four time periods, their absolute concentrations and contributions to OM varied considerably. The differences between the periods were driven by a combination of factors affecting isoprene SOA formation which included isoprene and NO_x mixing ratios (Kroll et al., 2006), aerosol acidity (Surratt et al., 2007, 2008), and relative humidity (Nguyen et al., 2011; Zhang et al., 2011). Throughout the study period, aerosol acidity (average pH of 1.9 ± 0.2) was consistent with previous estimates of aerosol pH in the Midwestern US (Pye et al., 2020).

The lowest organosulfate concentrations, on average, were observed during ozone period A when organosulfur species accounted for 1.4 ± 0.3% OM. Air masses from the upper Midwestern US (Fig. S3) brought

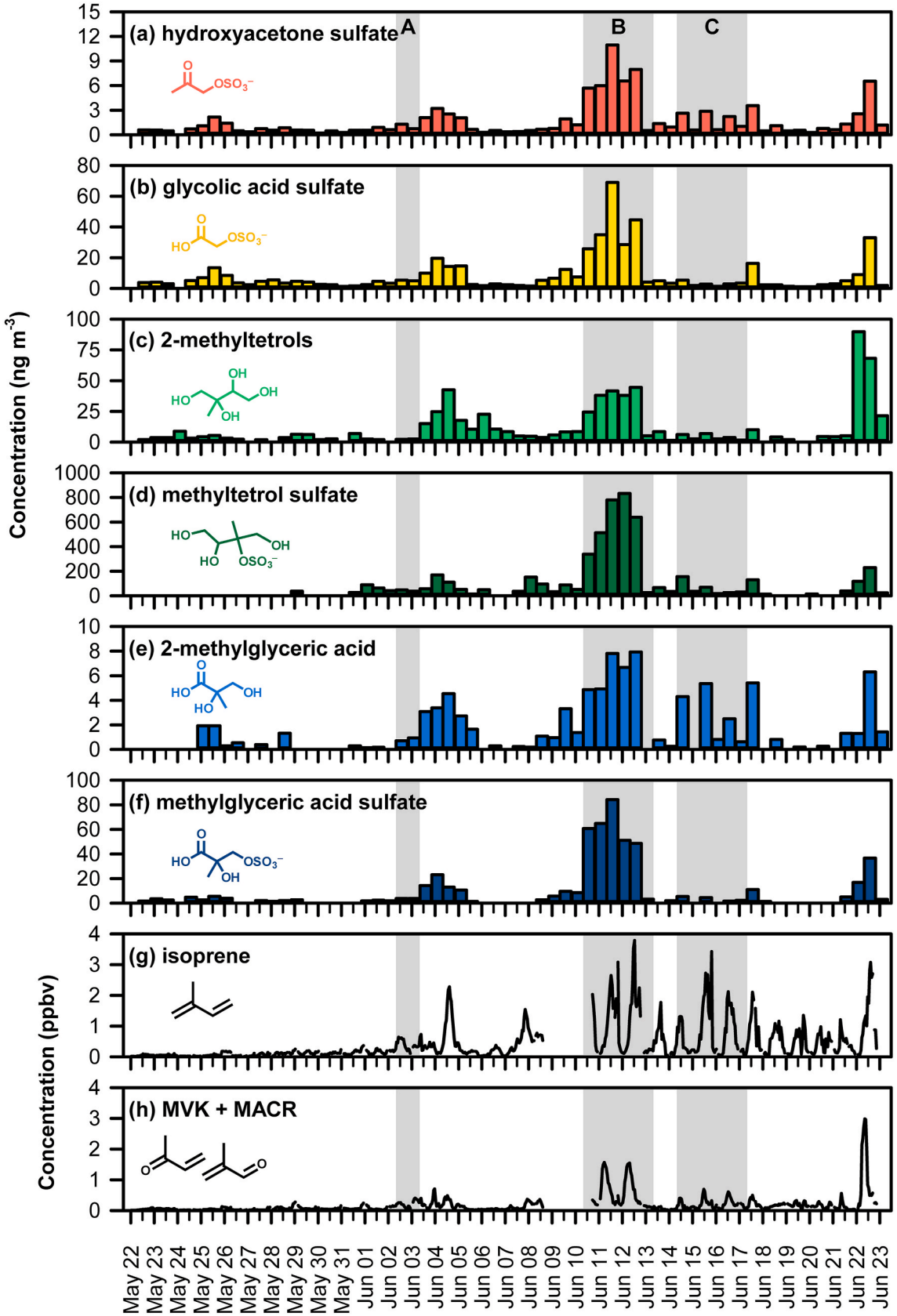

Fig. 3. Concentrations of (a) hydroxyacetone sulfate, (b) glycolic acid sulfate, (c) 2-methyltetrols, (d) methyltetrol sulfate, (e) 2-methylglyceric acid, (f) methylglyceric acid sulfate, (g) isoprene, and (h) methyl vinyl ketone and methacrolein (MVK + MACR) throughout the study period. Dates are defined using local time (CDT).

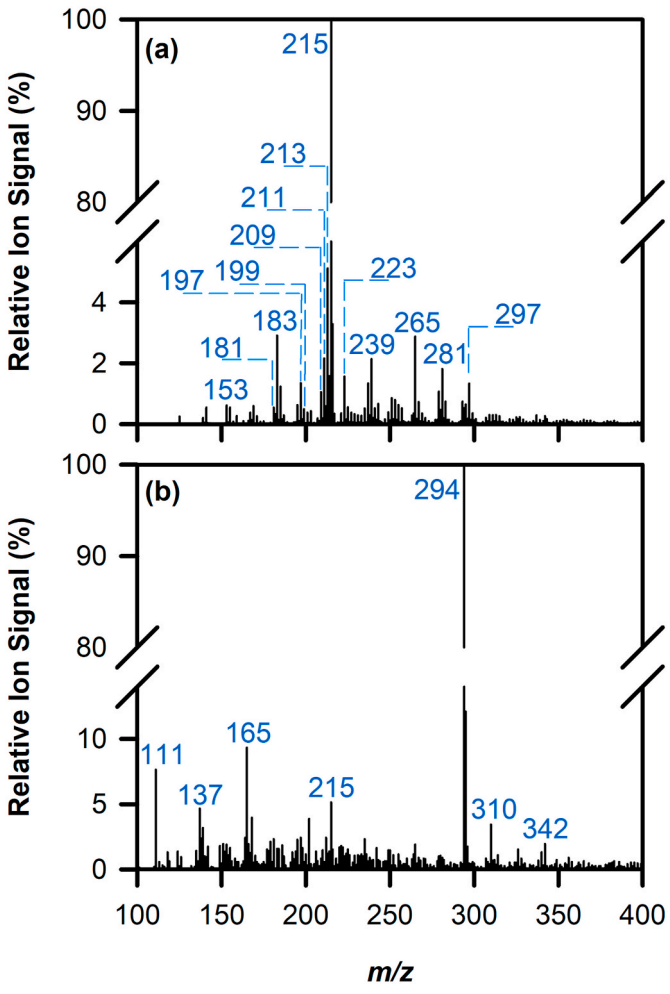

Fig. 4. Mass spectra corresponding to organosulfate species that fragment to the (a) bisulfate anion (*m/z* 97) and (b) sulfate ion radical (*m/z* 96). Stronger signals were obtained for the *m/z* 97 precursor ions relative to *m/z* 96 as demonstrated by maximum absolute signal of 146 700 au and 1883 au, respectively.

lower temperatures (20.1 °C on average) and lower isoprene mixing ratios (daytime peak: 0.99 ppbv). Although sulfate and NO_x concentrations were elevated, the aerosol was not as acidic as later ozone periods (Fig. 2). Together, these conditions resulted in little isoprene SOA formation.

Organosulfate concentrations increased 8-fold in period B and accounted for 15 ± 2% OM (Fig. 2 and Table 2). Southerly air masses (Fig. S4) from forested areas of Missouri and Arkansas increased the temperature and had higher isoprene mixing ratios (Fig. 3g; daytime peak: 5.84 ppbv). The co-occurrence of MVK and MACR (Fig. 3h) indicated photochemical aging. Higher sulfate concentrations (Table 1) and a lower relative humidity (Fig. S2c) combined to produce more acidic aerosol (Fig. 2d). The 8-fold increase in organosulfates during period B was attributed to a combination of these factors. Similar conditions were observed on 22 June, when air masses from the Southern US (Fig. S6) were transported to Zion along with elevated isoprene (Fig. 3g), sulfate (Fig. 1a), and aerosol acidity (pH −1.30). The 8-fold drop in organosulfate concentrations on the evening of 22 June was attributed to rainfall. Together, period B and 22 June reveal that periods with southerly winds and elevated temperatures, isoprene mixing ratios, and acidity are the most conducive to isoprene SOA in Zion.

A substantial reduction in isoprene SOA was observed at the end of ozone period B between the daytime and nighttime on 12 June as organosulfate concentrations decreased from 908 to 64 ng m^{-3}, respectively (Fig. 3). This decrease was attributed to enhanced particle dispersion and dilution (Cugerone et al., 2018; Wang and Ogawa, 2015) resulting from strong wind gusts (reaching 8 m s^{-1}) at 20:00 (CDT). Following the evening of 12 June, the concentration of organosulfates remained low throughout ozone period C when the origin of air masses shifted from the Southern US to the Midwestern US (Fig. S5) decreasing the temperature while increasing the relative humidity (Fig. S2) and lowering aerosol acidity (Fig. 2d). Isoprene mixing ratios were elevated (peaking at 4.92 ppbv), while MVK and MACR were low (Fig. 3h), indicating that isoprene was not very photochemically aged. This suggests that either the isoprene was emitted nearby and/or that the rate of photooxidation was slower relative to period B. Along with greater NO_x concentrations (Fig. 2d), relatively high concentrations of hydroxyacetone sulfate (Fig. 3a) and 2-methylglyceric acid (Fig. 3e) were observed, both of which form from oxidation of MACR under high-NO_x conditions (Lin et al., 2013; Schindelka et al., 2013). Though enhancements were observed for 2-methylgyceric acid, no commensurate increase was observed for 2-methylgyceric acid sulfate. Likewise, 2-methyltetrol sulfate did not increase. The low organosulfate concentrations throughout period C were attributed to the lower concentrations of inorganic sulfate (Table 1), higher relative humidity (Fig. 2d), and slightly less acidic aerosol (pH of 1.1 in C compared to 0.9 in B).

On 4 June, ozone was briefly elevated, reaching 71 ppbv between 14:00–16:00 concurrent with a northern lake breeze (Fig. S7). Relative to ozone period A and C, organosulfate concentrations increased two-fold and accounted for 4.5 ± 0.2% OM. Between 08:00–14:00 (CDT) on 4 June, air masses were transported from southern Missouri (Fig. S7) and resulted in an elevated temperature (23.1 °C) and isoprene mixing ratio (daytime peak: 3.65 ppbv). Notably, beginning at 14:00 and continuing through the nighttime, air masses were transported from the upper Midwestern US out over Lake Michigan and then delivered to Zion via a northerly lake breeze (Fig. S7). Compared to ozone period B, the 4 June had a similar concentration of sulfate (accounting for 15 ± 5% $PM_{2.5}$ mass) but a much lower aerosol acidity (pH of 2.41) coincident with a higher relative humidity (69% on 4 June versus 53% during period B). Much like period C, the concentrations of MVK and MACR on 4 June were relatively low (Fig. 3h) indicating that isoprene was oxidized to a lesser degree. This day provides a unique example of elevated SOA in air masses from northern Lake Michigan and further underscores the importance of sulfate, relative humidity, and aerosol pH on SOA formation.

3.5. *Comparison of organosulfates in LMOS 2017 to other locations in the US and globally*

The major isoprene-derived organosulfates identified in this study (*m/z* 215, 213, 211) are consistent with those detected during summertime at other locations, both by the same precursor ion scan MS/MS methods (Hettiyadura et al., 2017, 2019; Hughes and Stone, 2019) and by high-resolution MS (Brüggemann et al., 2020; Meade et al., 2016; Rattanavaraha et al., 2016; Wang et al., 2018). Furthermore, the majority of organosulfates being from isoprene is consistent with previous work in the Southeastern US (Hettiyadura et al., 2019; Rattanavaraha et al., 2016; Surratt et al., 2008), Denmark (Kristensen et al., 2016; Nguyen et al., 2014), Brazil (Glasius et al., 2018), and China (Ma et al., 2014; Wang et al., 2018). Among the isoprene-derived organosulfates, methyltetrol sulfate was estimated to account for 1.1% OC in Zion on average and up to 5.4% of OC during ozone period B. As a point of comparison, methyltetrol sulfate contributions to OC in locations heavily impacted by isoprene SOA during summertime were Centreville, Alabama (6.1%; Hettiyadura et al., 2017), Atlanta, Georgia (12.6%; Hettiyadura et al., 2019), and Look Rock, Tennessee (12.9%; Cui et al., 2018), with more moderate impacts in Iowa City, Iowa (3.4%; Hughes and Stone, 2019), and lesser impacts in Manaus, Brazil (1.3%; Glasius et al., 2018), Towson, Maryland (0.04%; Meade et al., 2016), and Changping, China (0.02%; Wang et al., 2018). The elevated methyltetrol

Table 3
Organosulfates identified in Zion, IL from the precursor to *m/z* 97 scan. Summarized for each compound is the calculated monoisotopic mass, formula determined by TOF-MS, proposed structure, VOC precursor(s) with references to prior studies, HILIC retention time for major peaks, *m/z* error, and the percent contribution to the precursor ion signal.

Calculated Mass [M-H]$^-$	Formula	Proposed Structure	VOC Precursor(s)	t_R (min.)	Error (mDa)	Contribution to precursorion signal (%)
215.0225 methyltetrol sulfate	$C_5H_{11}SO_7^-$	[a] 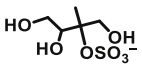	Isoprene[a-b]	1.30 1.58 2.45 3.03	0.3 0.4 −0.4 −0.1	54.4
213.0069	$C_5H_9SO_7^-$	[c] 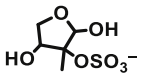	Isoprene[b]	1.03 1.36 1.98	0.2 0.4 −0.4	2.8
182.9963	$C_4H_7SO_6^-$	[d] 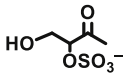	Isoprene[e] MVK/MACR[f-g]	0.86 0.99	−0.3 −0.9	1.4
239.0225	$C_7H_{11}SO_7^-$	[h] 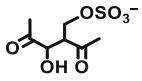	Limonene[b] MVK/MACR[h]	0.71	0.5	1.2
265.1474	$C_{12}H_{25}SO_4^-$	[i] 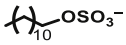	Anthropogenic[i]	0.52	−0.6	1.2
210.9912	$C_5H_7SO_7^-$	[c] 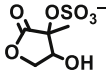	Isoprene[b]	0.52 0.67 0.81	1.6 0.6 0.3	1.0
197.0120	$C_5H_9SO_6^-$	[e] 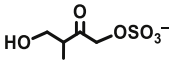	Isoprene[e]	0.56 0.90	−0.5 −0.6	0.43
181.0171	$C_5H_9SO_5^-$	[e] 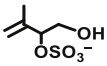	Isoprene[e]	0.60 0.76	−0.1 0.5	0.25
199.0276	$C_5H_{11}SO_6^-$	[j] 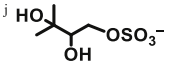	Isoprene[e] MBO[j-k]	1.69	−0.7	0.16
198.9912 methylglyceric acid sulfate	$C_4H_7SO_7^-$	[b] 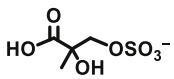	Isoprene[l]	7.71	3.7	0.1
294.0647[m]	$C_{10}H_{16}NSO_7^-$	[b] 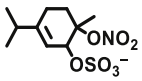	α-pinene[n]	0.55	0.2	29.1
164.9858[m]	$C_4H_5SO_5^-$	[o] 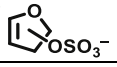	Cyclohexene[p]	0.64	−1.0	2.4

[a] Surratt et al. (2010); [b] Surratt et al. (2008); [c] Hettiyadura et al. (2015); [d] Shalamzari et al. (2014); [e] Riva et al. (2016); [f] methyl vinyl ketone (MVK) methacrolein (MACR); [g] Schindelka et al. (2013); [h] Nozière et al. (2010); [i] Hettiyadura et al. (2017); [j] Zhang et al. (2012); [k] 2-methyl-3-buten-2-ol (MBO); [l] Gómez-González et al. (2008); [m] Identified in precursor to *m/z* 96 scan; [n] Iinuma et al. (2007a); [o] Hettiyadura et al. (2019); [p] Liu et al. (2017).

sulfate concentrations in period B (averaging 520 ng m^{-3}) approached those observed in at a remote location in the Southeastern US (Centreville, Alabama; averaging 670 ng m^{-3}) (Hettiyadura et al., 2017, 2019). Together, these data indicate a moderate influence of isoprene SOA in Zion across the LMOS study, with exceptionally high impacts occurring in period B.

4. Conclusions

Through quantitative measurements of organosulfates during summertime, we shed new light on the episodic nature of biogenic SOA in the Midwestern US. Under conditions of anthropogenic sulfate, high biogenic VOC concentrations, and acidic aerosol particles that were accompanied by southerly winds, the absolute concentrations of isoprene-derived organosulfates approached levels observed at the remote Centreville, Alabama site in the Southeastern U.S. during summertime (Hettiyadura et al., 2017, 2019). These data demonstrate that SOA periodically has a substantial impact on $PM_{2.5}$ in the Upper Midwestern US and that on occasion, high SOA coincides with elevated PM and ozone levels.

Furthermore, this study provides insight into the relationship between $PM_{2.5}$ composition and ozone along the Lake Michigan coastline during LMOS 2017. Three periods of elevated ozone each corresponded to distinct $PM_{2.5}$ concentrations and composition. Ozone period A was an episode of elevated ozone with a clear influence from coastal meteorology where the wind dramatically shifted from south-westerly to a south-easterly lake breeze that persisted for ten hours. Relative to the other days throughout LMOS 2017, period A was unique in that $PM_{2.5}$ composition was more heavily influenced by primary combustion sources. Ozone period B was influenced by interstate transport from forested areas to the south and southwest, with a high influence from SOA production and a significant mass concentration of organosulfates. Ozone period C was distinctly different from period B due to variable wind directions, higher NO_x concentrations, and less acidic aerosol. Taken together, the chemical signatures of $PM_{2.5}$ and back trajectories during these coastal Lake Michigan ozone episodes show variation in chemical histories and source regions from episode to episode. The chemical measurements described herein provide initial insight to the sources of $PM_{2.5}$ during LMOS 2017, with source apportionment of $PM_{2.5}$ to follow.

Funding

This work was funded by the National Science Foundation under grants AGS-1405014, AGS-1712909, AGS-1713001, and AGS-1712828. DBM and HDA also acknowledge support from NSF under grant AGS-1428257.

Data availability

All field data from LMOS 2017 including the chemical and meteorological measurements presented in this manuscript are available on the NASA LaRC data archive (https://www-air.larc.nasa.gov/cgi-bin/ArcView/lmos).

CRediT authorship contribution statement

Dagen D. Hughes: Methodology, Validation, Formal analysis, Investigation, Data curation, Writing - original draft, Writing - review & editing, Visualization. **Megan B. Christiansen:** Formal analysis, Investigation, Writing - original draft, Writing - review & editing. **Alissa Milani:** Investigation, Writing - review & editing. **Michael P. Vermeuel:** Investigation, Writing - review & editing. **Gordon A. Novak:** Investigation, Writing - review & editing. **Hariprasad D. Alwe:** Investigation, Writing - review & editing. **Angela F. Dickens:** Writing - review & editing, Project administration. **R. Bradley Pierce:** Writing - review & editing, Project administration. **Dylan B. Millet:** Conceptualization, Investigation, Writing - review & editing, Project administration, Funding acquisition. **Timothy H. Bertram:** Conceptualization, Investigation, Writing - review & editing, Project administration, Funding acquisition. **Charles O. Stanier:** Conceptualization, Investigation, Formal analysis, Writing - review & editing, Project administration, Funding acquisition. **Elizabeth A. Stone:** Conceptualization, Methodology, Investigation, Writing - review & editing, Supervision, Project administration, Funding acquisition.

Declaration of competing interest

The authors declare that they have no known competing financial interests or personal relationships that could have appeared to influence the work reported in this paper.

Acknowledgements

The authors would like to thank everyone involved with LMOS 2017. We would also like to thank Lynn Teesch and Vic Parcell of the University of Iowa High-Resolution Mass Spectrometry Facility for their assistance with instrumentation.

Appendix A. Supplementary data

Supplementary data to this article can be found online at https://doi.org/10.1016/j.atmosenv.2020.117939.

References

Abdi-Oskouei, M., Carmichael, G., Christiansen, M., Ferrada, G., Roozitalab, B., Sobhani, N., Wade, K., Czarnetzki, A., Pierce, R.B., Wagner, T., Stanier, C., 2020. Sensitivity of meteorological skill to selection of WRF-chem physical parameterizations and impact on ozone prediction during the lake Michigan ozone study (LMOS). J. Geophys. Res. Atmos. 125, e2019JD031971 https://doi.org/10.1029/2019jd031971.

Al-Naiema, I.M., Stone, E.A., 2017. Evaluation of anthropogenic secondary organic aerosol tracers from aromatic hydrocarbons. Atmos. Chem. Phys. 17, 2053–2065. https://doi.org/10.5194/acp-17-2053-2017.

Allen, D.T., Turner, J.R., 2008. Transport of atmospheric fine particulate matter: Part 1—findings from recent field programs on the extent of regional transport within north America. J. Air Waste Manag. Assoc. 58, 254–264. https://doi.org/10.3155/1047-3289.58.2.254.

Angevine, W.M., Senff, C.J., White, A.B., Williams, E.J., Koermer, J., Miller, S.T.K., Talbot, R., Johnston, P.E., Mckeen, S.A., Downs, T., 2004. Coastal boundary layer influence on pollutant transport in new England. J. Appl. Meteorol. 43, 1425–1437. https://doi.org/10.1175/jam2148.1.

Atkinson, R., 2000. Atmospheric chemistry of VOCs and NOx. Atmos. Environ. 34, 2063–2101. https://doi.org/10.1016/S1352-2310(99)00460-4.

Attygalle, A.B., Garcā-a-Rubio, S., Ta, J., Meinwald, J., 2001. Collisionally-induced dissociation mass spectra of organic sulfate anions. J. Chem. Soc., Perkin Trans. 2, 498–506. https://doi.org/10.1039/B009019K.

Aw, J., Kleeman, M.J., 2003. Evaluating the first-order effect of intraannual temperature variability on urban air pollution. J. Geophys. Res. Atmos. 108 https://doi.org/10.1029/2002jd002688.

Banta, R.M., Senff, C.J., Alvarez, R.J., Langford, A.O., Parrish, D.D., Trainer, M.K., Darby, L.S., Hardesty, R.M., Lambeth, B., Neuman, J.A., 2011. Dependence of daily peak O3 concentrations near Houston, Texas on environmental factors: wind speed, temperature, and boundary-layer depth. Atmos. Environ. 45, 162–173. https://doi.org/10.1016/j.atmosenv.2010.09.030.

Bertram, T.H., Kimmel, J.R., Crisp, T.A., Ryder, O.S., Yatavelli, R.L.N., Thornton, J.A., Cubison, M.J., Gonin, M., Worsnop, D.R., 2011. A field-deployable, chemical ionization time-of-flight mass spectrometer. Atmos. Meas. Tech. 4, 1471–1479. https://doi.org/10.5194/amt-4-1471-2011.

Brüggemann, M., Xu, R., Tilgner, A., Kwong, K.C., Mutzel, A., Poon, H.Y., Otto, T., Schaefer, T., Poulain, L., Chan, M.N., Herrmann, H., 2020. Organosulfates in ambient aerosol: state of knowledge and future Research directions on formation, abundance, fate, and importance. Environ. Sci. Technol. 54, 3767–3782. https://doi.org/10.1021/acs.est.9b06751.

Budisulistiorini, S.H., Li, X., Bairai, S.T., Renfro, J., Liu, Y., Liu, Y.J., Mckinney, K.A., Martin, S.T., Mcneill, V.F., Pye, H.O.T., Nenes, A., Neff, M.E., Stone, E.A., Mueller, S., Knote, C., Shaw, S.L., Zhang, Z., Gold, A., Surratt, J.D., 2015. Examining the effects of anthropogenic emissions on isoprene-derived secondary organic aerosol formation during the 2013 Southern Oxidant and Aerosol Study (SOAS) at the Look Rock, Tennessee ground site. Atmos. Chem. Phys. 15, 8871–8888. https://doi.org/10.5194/acp-15-8871-2015.

Bullard, R.L., Singh, A., Anderson, S.M., Lehmann, C.M.B., Stanier, C.O., 2017. 10-Month characterization of the aerosol number size distribution and related air quality and meteorology at the Bondville, IL Midwestern background site. Atmos. Environ. 154, 348–361. https://doi.org/10.1016/j.atmosenv.2016.12.055.

Buzcu-Guven, B., Brown, S.G., Frankel, A., Hafner, H.R., Roberts, P.T., 2007. Analysis and apportionment of organic carbon and fine particulate matter sources at multiple sites in the Midwestern United States. J. Air Waste Manag. Assoc. 57, 606–619. https://doi.org/10.3155/1047-3289.57.5.606.

Cabada, J.C., Pandis, S.N., Subramanian, R., Robinson, A.L., Polidori, A., Turpin, B., 2004. Estimating the secondary organic aerosol contribution to PM2.5 using the EC tracer method special issue of aerosol science and technology on findings from the fine particulate matter supersites program. Aerosol Sci. Technol. 38, 140–155. https://doi.org/10.1080/02786820390229084.

Carlton, A.G., Pinder, R.W., Bhave, P.V., Pouliot, G.A., 2010. To what extent can biogenic SOA be controlled? Environ. Sci. Technol. 44, 3376–3380. https://doi.org/10.1021/es903506b.

Carlton, A.G., Wiedinmyer, C., Kroll, J.H., 2009. A review of Secondary Organic Aerosol (SOA) formation from isoprene. Atmos. Chem. Phys. 9, 4987–5005. https://doi.org/10.5194/acp-9-4987-2009.

Chan, M.N., Surratt, J.D., Chan, A.W.H., Schilling, K., Offenberg, J.H., Lewandowski, M., Edney, E.O., Kleindienst, T.E., Jaoui, M., Edgerton, E.S., Tanner, R.L., Shaw, S.L., Zheng, M., Knipping, E.M., Seinfeld, J.H., 2011. Influence of aerosol acidity on the chemical composition of secondary organic aerosol from β-caryophyllene. Atmos. Chem. Phys. 11, 1735–1751. https://doi.org/10.5194/acp-11-1735-2011.

Cortés-Francisco, N., Caixach, J., 2013. Molecular characterization of dissolved organic matter through a desalination process by high resolution mass spectrometry. Environ. Sci. Technol. 47, 9619–9627. https://doi.org/10.1021/es4000388.

Cugerone, K., De Michele, C., Ghezzi, A., Gianelle, V., 2018. Aerosol removal due to precipitation and wind forcings in Milan urban area. J. Hydrol. 556, 1256–1262. https://doi.org/10.1016/j.jhydrol.2017.06.033.

Cui, T., Zeng, Z., Dos Santos, E.O., Zhang, Z., Chen, Y., Zhang, Y., Rose, C.A., Budisulistiorini, S.H., Collins, L.B., Bodnar, W.M., De Souza, R.a.F., Martin, S.T., Machado, C.M.D., Turpin, B.J., Gold, A., Ault, A.P., Surratt, J.D., 2018. Development of a hydrophilic interaction liquid chromatography (HILIC) method for the chemical characterization of water-soluble isoprene epoxydiol (IEPOX)-derived secondary organic aerosol. Environ. Sci.: Processes Impacts 20, 1524–1536. https://doi.org/10.1039/C8EM00308D.

Darer, A.I., Cole-Filipiak, N.C., O'connor, A.E., Elrod, M.J., 2011. Formation and stability of atmospherically relevant isoprene-derived organosulfates and organonitrates. Environ. Sci. Technol. 45, 1895–1902. https://doi.org/10.1021/es103797z.

De Gouw, J.A., Middlebrook, A.M., Warneke, C., Goldan, P.D., Kuster, W.C., Roberts, J. M., Fehsenfeld, F.C., Worsnop, D.R., Canagaratna, M.R., Pszenny, A.a.P., Keene, W. C., Marchewka, M., Bertman, S.B., Bates, T.S., 2005. Budget of organic carbon in a polluted atmosphere: results from the new England air quality study in 2002. J. Geophys. Res. Atmos. 110 https://doi.org/10.1029/2004jd005623.

Dye, T.S., Roberts, P.T., Korc, M.E., 1995. Observations of transport processes for ozone and ozone precursors during the 1991 lake Michigan ozone study. J. Appl. Meteorol. 34, 1877–1889. https://doi.org/10.1175/1520-0450(1995)034<1877:ootpfo>2.0.co;2.

Fosco, T., Schmeling, M., 2007. Determination of water-soluble atmospheric aerosols using ion chromatography. Environ. Monit. Assess. 130, 187–199. https://doi.org/10.1007/s10661-006-9388-1.

Glasius, M., Bering, M.S., Yee, L.D., De Sá, S.S., Isaacman-Vanwertz, G., Wernis, R.A., Barbosa, H.M.J., Alexander, M.L., Palm, B.B., Hu, W., Campuzano-Jost, P., Day, D.A., Jimenez, J.L., Shrivastava, M., Martin, S.T., Goldstein, A.H., 2018. Organosulfates in aerosols downwind of an urban region in central Amazon. Environ. Sci.: Processes Impacts 20, 1546–1558. https://doi.org/10.1039/C8EM00413G.

Gómez-González, Y., Surratt, J.D., Cuyckens, F., Szmigielski, R., Vermeylen, R., Jaoui, M., Lewandowski, M., Offenberg, J.H., Kleindienst, T.E., Edney, E.O., Blockhuys, F., Van Alsenoy, C., Maenhaut, W., Claeys, M., 2008. Characterization of organosulfates from the photooxidation of isoprene and unsaturated fatty acids in

ambient aerosol using liquid chromatography/(−) electrospray ionization mass spectrometry. J. Mass Spectrom. 43, 371–382. https://doi.org/10.1002/jms.1329.
Guenther, A.B., Jiang, X., Heald, C.L., Sakulyanontvittaya, T., Duhl, T., Emmons, L.K., Wang, X., 2012. The Model of Emissions of Gases and Aerosols from Nature version 2.1 (MEGAN2.1): an extended and updated framework for modeling biogenic emissions. Geosci. Model Dev. 5, 1471–1492. https://doi.org/10.5194/gmd-5-1471-2012.
Hallquist, M., Wenger, J.C., Baltensperger, U., Rudich, Y., Simpson, D., Claeys, M., Dommen, J., Donahue, N.M., George, C., Goldstein, A.H., Hamilton, J.F., Herrmann, H., Hoffmann, T., Iinuma, Y., Jang, M., Jenkin, M.E., Jimenez, J.L., Kiendler-Scharr, A., Maenhaut, W., Mcfiggans, G., Mentel, T.F., Monod, A., Prévôt, A.S.H., Seinfeld, J.H., Surratt, J.D., Szmigielski, R., Wildt, J., 2009. The formation, properties and impact of secondary organic aerosol: current and emerging issues. Atmos. Chem. Phys. 9, 5155–5236. https://doi.org/10.5194/acp-9-5155-2009.
Harris, L., Kotamarthi, V.R., 2005. The characteristics of the Chicago lake breeze and its effects on trace particle transport: results from an episodic event simulation. J. Appl. Meteorol. 44, 1637–1654. https://doi.org/10.1175/jam2301.1.
Hastie, D.R., Narayan, J., Schiller, C., Niki, H., Shepson, P.B., Sills, D.M.L., Taylor, P.A., Moroz, W.J., Drummond, J.W., Reid, N., Taylor, R., Roussel, P.B., Melo, O.T., 1999. Observational evidence for the impact of the lake breeze circulation on ozone concentrations in Southern Ontario. Atmos. Environ. 33, 323–335. https://doi.org/10.1016/S1352-2310(98)00199-X.
Haywood, J., Boucher, O., 2000. Estimates of the direct and indirect radiative forcing due to tropospheric aerosols: a review. Rev. Geophys. 38, 513–543. https://doi.org/10.1029/1999RG000078.
Henze, D.K., Seinfeld, J.H., 2006. Global secondary organic aerosol from isoprene oxidation. Geophys. Res. Lett. 33 https://doi.org/10.1029/2006gl025976.
Hettiyadura, A.P.S., Al-Naiema, I.M., Hughes, D.D., Fang, T., Stone, E.A., 2019. Organosulfates in Atlanta, Georgia: anthropogenic influences on biogenic secondary organic aerosol formation. Atmos. Chem. Phys. 19, 3191–3206. https://doi.org/10.5194/acp-19-3191-2019.
Hettiyadura, A.P.S., Jayarathne, T., Baumann, K., Goldstein, A.H., De Gouw, J.A., Koss, A., Keutsch, F.N., Skog, K., Stone, E.A., 2017. Qualitative and quantitative analysis of atmospheric organosulfates in Centreville, Alabama. Atmos. Chem. Phys. 17, 1343–1359. https://doi.org/10.5194/acp-17-1343-2017.
Hettiyadura, A.P.S., Stone, E.A., Kundu, S., Baker, Z., Geddes, E., Richards, K., Humphry, T., 2015. Determination of atmospheric organosulfates using HILIC chromatography with MS detection. Atmos. Meas. Tech. 8, 2347–2358. https://doi.org/10.5194/amt-8-2347-2015.
Hopke, P.K., 2016. Review of receptor modeling methods for source apportionment. J. Air Waste Manag. Assoc. 66, 237–259. https://doi.org/10.1080/10962247.2016.1140693.
Hughes, D.D., Stone, E.A., 2019. Organosulfates in the Midwestern United States: abundance, composition and stability. Environ. Chem. 16, 312–322. https://doi.org/10.1071/EN18260.
Iinuma, Y., Boge, O., Kahnt, A., Herrmann, H., 2009. Laboratory chamber studies on the formation of organosulfates from reactive uptake of monoterpene oxides. Phys. Chem. Chem. Phys. 11, 7985–7997. https://doi.org/10.1039/B904025K.
Iinuma, Y., Müller, C., Berndt, T., Böge, O., Claeys, M., Herrmann, H., 2007a. Evidence for the existence of organosulfates from β-pinene ozonolysis in ambient secondary organic aerosol. Environ. Sci. Technol. 41, 6678–6683. https://doi.org/10.1021/es070938t.
Iinuma, Y., Müller, C., Böge, O., Gnauk, T., Herrmann, H., 2007b. The formation of organic sulfate esters in the limonene ozonolysis secondary organic aerosol (SOA) under acidic conditions. Atmos. Environ. 41, 5571–5583. https://doi.org/10.1016/j.atmosenv.2007.03.007.
Jayarathne, T., Rathnayake, C.M., Stone, E.A., 2016. Local source impacts on primary and secondary aerosols in the Midwestern United States. Atmos. Environ. 130, 74–83. https://doi.org/10.1016/j.atmosenv.2015.09.058.
Jayarathne, T., Stockwell, C.E., Yokelson, R.J., Nakao, S., Stone, E.A., 2014. Emissions of fine particle fluoride from biomass burning. Environ. Sci. Technol. 48, 12636–12644. https://doi.org/10.1021/es502933j.
Jeong, C.H., Mcguire, M.L., Godri, K.J., Slowik, J.G., Rehbein, P.J.G., Evans, G.J., 2011. Quantification of aerosol chemical composition using continuous single particle measurements. Atmos. Chem. Phys. 11, 7027–7044. https://doi.org/10.5194/acp-11-7027-2011.
Jin, X., Wang, Y., Li, Z., Zhang, F., Xu, W., Sun, Y., Fan, X., Chen, G., Wu, H., Ren, J., Wang, Q., Cribb, M., 2020. Significant contribution of organics to aerosol liquid water content in winter in Beijing, China. Atmos. Chem. Phys. 20, 901–914. https://doi.org/10.5194/acp-20-901-2020.
Kampa, M., Castanas, E., 2008. Human health effects of air pollution. Environ. Pollut. 151, 362–367. https://doi.org/10.1016/j.envpol.2007.06.012.
Kanakidou, M., Seinfeld, J.H., Pandis, S.N., Barnes, I., Dentener, F.J., Facchini, M.C., Van Dingenen, R., Ervens, B., Nenes, A., Nielsen, C.J., Swietlicki, E., Putaud, J.P., Balkanski, Y., Fuzzi, S., Horth, J., Moortgat, G.K., Winterhalter, R., Myhre, C.E.L., Tsigaridis, K., Vignati, E., Stephanou, E.G., Wilson, J., 2005. Organic aerosol and global climate modelling: a review. Atmos. Chem. Phys. 5, 1053–1123. https://doi.org/10.5194/acp-5-1053-2005.
Kim, E., Hopke, P.K., Kenski, D.M., Koerber, M., 2005. Sources of fine particles in a Rural Midwestern U.S. Area. Environ. Sci. Technol. 39, 4953–4960. https://doi.org/10.1021/es0490774.
Kristensen, K., Bilde, M., Aalto, P.P., Petäjä, T., Glasius, M., 2016. Denuder/filter sampling of organic acids and organosulfates at urban and boreal forest sites: gas/particle distribution and possible sampling artifacts. Atmos. Environ. 130, 36–53. https://doi.org/10.1016/j.atmosenv.2015.10.046.
Kroll, J.H., Ng, N.L., Murphy, S.M., Flagan, R.C., Seinfeld, J.H., 2006. Secondary organic aerosol formation from isoprene photooxidation. Environ. Sci. Technol. 40, 1869–1877. https://doi.org/10.1021/es0524301.
Lee, J.H., Hopke, P.K., 2006. Apportioning sources of PM2.5 in St. Louis, MO using speciation trends network data. Atmos. Environ. 40, 360–377. https://doi.org/10.1016/j.atmosenv.2005.11.074.
Li, K., Jacob, D.J., Liao, H., Shen, L., Zhang, Q., Bates, K.H., 2019. Anthropogenic drivers of 2013–2017 trends in summer surface ozone in China. Proc. Natl. Acad. Sci. U.S.A. 116, 422–427. https://doi.org/10.1073/pnas.1812168116.
Liao, J., Froyd, K.D., Murphy, D.M., Keutsch, F.N., Yu, G., Wennberg, P.O., St Clair, J.M., Crounse, J.D., Wisthaler, A., Mikoviny, T., Jimenez, J.L., Campuzano-Jost, P., Day, D.A., Hu, W., Ryerson, T.B., Pollack, I.B., Peischl, J., Anderson, B.E., Ziemba, L. D., Blake, D.R., Meinardi, S., Diskin, G., 2015. Airborne measurements of organosulfates over the continental U.S. J. Geophys. Res.: Atmos. 120, 2990–3005. https://doi.org/10.1002/2014JD022378.
Lim, H.J., Turpin, B.J., Russell, L.M., Bates, T.S., 2003. Organic and elemental carbon measurements during ACE-Asia suggest a longer atmospheric lifetime for elemental carbon. Environ. Sci. Technol. 37, 3055–3061. https://doi.org/10.1021/es020988s.
Lin, Y.-H., Zhang, H., Pye, H.O.T., Zhang, Z., Marth, W.J., Park, S., Arashiro, M., Cui, T., Budisulistiorini, S.H., Sexton, K.G., Vizuete, W., Xie, Y., Luecken, D.J., Piletic, I.R., Edney, E.O., Bartolotti, L.J., Gold, A., Surratt, J.D., 2013. Epoxide as a precursor to secondary organic aerosol formation from isoprene photooxidation in the presence of nitrogen oxides. Proc. Natl. Acad. Sci. U.S.A. 110, 6718–6723. https://doi.org/10.1073/pnas.1221150110.
Liu, S., Jia, L., Xu, Y., Tsona, N.T., Ge, S., Du, L., 2017. Photooxidation of cyclohexene in the presence of SO2: SOA yield and chemical composition. Atmos. Chem. Phys. 17, 13329–13343. https://doi.org/10.5194/acp-17-13329-2017.
Loughner, C.P., Tzortziou, M., Follette-Cook, M., Pickering, K.E., Goldberg, D., Satam, C., Weinheimer, A., Crawford, J.H., Knapp, D.J., Montzka, D.D., Diskin, G.S., Dickerson, R.R., 2014. Impact of bay-breeze circulations on surface air quality and boundary layer export. J. Appl. Meteorol. Climatol. 53, 1697–1713. https://doi.org/10.1175/jamc-d-13-0323.1.
Ma, Y., Xu, X., Song, W., Geng, F., Wang, L., 2014. Seasonal and diurnal variations of particulate organosulfates in urban Shanghai, China. Atmos. Environ 85, 152–160. https://doi.org/10.1016/j.atmosenv.2013.12.017.
Meade, L.E., Riva, M., Blomberg, M.Z., Brock, A.K., Qualters, E.M., Siejack, R.A., Ramakrishnan, K., Surratt, J.D., Kautzman, K.E., 2016. Seasonal variations of fine particulate organosulfates derived from biogenic and anthropogenic hydrocarbons in the mid-Atlantic United States. Atmos. Environ 145, 405–414. https://doi.org/10.1016/j.atmosenv.2016.09.028.
Meng, Z., Dabdub, D., Seinfeld, J.H., 1997. Chemical coupling between atmospheric ozone and particulate matter. Science 277, 116–119. https://doi.org/10.1126/science.277.5322.116.
Millet, D.B., Alwe, H.D., Chen, X., Deventer, M.J., Griffis, T.J., Holzinger, R., Bertman, S. B., Rickly, P.S., Stevens, P.S., Léonardis, T., Locoge, N., Dusanter, S., Tyndall, G.S., Alvarez, S.L., Erickson, M.H., Flynn, J.H., 2018. Bidirectional ecosystem–atmosphere fluxes of volatile organic compounds across the mass spectrum: how many matter? ACS Earth Space Chem 2, 764–777. https://doi.org/10.1021/acsearthspacechem.8b00061.
Morishita, M., Keeler, G.J., Kamal, A.S., Wagner, J.G., Harkema, J.R., Rohr, A.C., 2011. Identification of ambient PM2.5 sources and analysis of pollution episodes in Detroit, Michigan using highly time-resolved measurements. Atmos. Environ. 45, 1627–1637. https://doi.org/10.1016/j.atmosenv.2010.09.062.
Nguyen, Q., Christensen, M.K., Cozzi, F., Zare, A., Hansen, A.M.K., Kristensen, K., Tulinius, T.E., Madsen, H., Christensen, J.H., Brandt, J., 2014. Understanding the anthropogenic influence on formation of biogenic secondary organic aerosols in Denmark via analysis of organosulfates and related oxidation products. Atmos. Chem. Phys. 14, 8961–8981. https://doi.org/10.5194/acp-14-8961-2014.
Nguyen, T.B., Bates, K.H., Crounse, J.D., Schwantes, R.H., Zhang, X., Kjaergaard, H.G., Surratt, J.D., Lin, P., Laskin, A., Seinfeld, J.H., Wennberg, P.O., 2015. Mechanism of the hydroxyl radical oxidation of methacryloyl peroxynitrate (MPAN) and its pathway toward secondary organic aerosol formation in the atmosphere. Phys. Chem. Chem. Phys. 17, 17914–17926. https://doi.org/10.1039/C5CP02001H.
Nguyen, T.B., Roach, P.J., Laskin, J., Laskin, A., Nizkorodov, S.A., 2011. Effect of humidity on the composition of isoprene photooxidation secondary organic aerosol. Atmos. Chem. Phys. 11, 6931–6944. https://doi.org/10.5194/acp-11-6931-2011.
Nozière, B., Ekström, S., Alsberg, T., Holmström, S., 2010. Radical-initiated formation of organosulfates and surfactants in atmospheric aerosols. Geophys. Res. Lett. 37 https://doi.org/10.1029/2009GL041683.
Olson, C.N., Galloway, M.M., Yu, G., Hedman, C.J., Lockett, M.R., Yoon, T., Stone, E.A., Smith, L.M., Keutsch, F.N., 2011. Hydroxycarboxylic acid-derived organosulfates: synthesis, stability, and quantification in ambient aerosol. Environ. Sci. Technol. 45, 6468–6474. https://doi.org/10.1021/es201039p.
Pancras, J.P., Landis, M.S., Norris, G.A., Vedantham, R., Dvonch, J.T., 2013. Source apportionment of ambient fine particulate matter in Dearborn, Michigan, using hourly resolved PM chemical composition data. Sci. Total Environ. 448, 2–13. https://doi.org/10.1016/j.scitotenv.2012.11.083.
Pierce, B., Kaleel, R., Dickens, A., Bertram, T., Stanier, C.O., Kenski, D.M., 2016. White paper: lake Michigan ozone study 2017. http://ladco.org/reports/ozone/post08/Great_Lakes_Ozone_Study_White_Paper_Draft_v6.pdf.
Pye, H.O.T., Nenes, A., Alexander, B., Ault, A.P., Barth, M.C., Clegg, S.L., Collett Jr., J.L., Fahey, K.M., Hennigan, C.J., Herrmann, H., Kanakidou, M., Kelly, J.T., Ku, I.T., Mcneill, V.F., Riemer, N., Schaefer, T., Shi, G., Tilgner, A., Walker, J.T., Wang, T., Weber, R., Xing, J., Zaveri, R.A., Zuend, A., 2020. The acidity of atmospheric particles and clouds. Atmos. Chem. Phys. 20, 4809–4888. https://doi.org/10.5194/acp-20-4809-2020.

Rattanavaraha, W., Chu, K., Budisulistiorini, S.H., Riva, M., Lin, Y.H., Edgerton, E.S., Baumann, K., Shaw, S.L., Guo, H., King, L., Weber, R.J., Neff, M.E., Stone, E.A., Offenberg, J.H., Zhang, Z., Gold, A., Surratt, J.D., 2016. Assessing the impact of anthropogenic pollution on isoprene-derived secondary organic aerosol formation in PM2.5 collected from the Birmingham, Alabama, ground site during the 2013 Southern oxidant and aerosol study. Atmos. Chem. Phys. 16, 4897–4914. https://doi.org/10.5194/acp-16-4897-2016.

Riva, M., Budisulistiorini, S.H., Zhang, Z., Gold, A., Surratt, J.D., 2016. Chemical characterization of secondary organic aerosol constituents from isoprene ozonolysis in the presence of acidic aerosol. Atmos. Environ. 130, 5–13. https://doi.org/10.1016/j.atmosenv.2015.06.027.

Rizzo, M.J., Scheff, P.A., 2007. Fine particulate source apportionment using data from the USEPA speciation trends network in Chicago, Illinois: comparison of two source apportionment models. Atmos. Environ. 41, 6276–6288. https://doi.org/10.1016/j.atmosenv.2007.03.055.

Rolph, G., Stein, A., Stunder, B., 2017. Real-time environmental Applications and Display sYstem: READY. Environ. Model. Software 95, 210–228. https://doi.org/10.1016/j.envsoft.2017.06.025.

Schauer, J.J., Mader, B.T., Deminter, J.T., Heidemann, G., Bae, M.S., Seinfeld, J.H., Flagan, R.C., Cary, R.A., Smith, D., Huebert, B.J., Bertram, T., Howell, S., Kline, J.T., Quinn, P., Bates, T., Turpin, B., Lim, H.J., Yu, J.Z., Yang, H., Keywood, M.D., 2003. ACE-asia intercomparison of a thermal-optical method for the determination of particle-phase organic and elemental carbon. Environ. Sci. Technol. 37, 993–1001. https://doi.org/10.1021/es020622f.

Schindelka, J., Iinuma, Y., Hoffmann, D., Herrmann, H., 2013. Sulfate radical-initiated formation of isoprene-derived organosulfates in atmospheric aerosols. Faraday Discuss 165, 237–259. https://doi.org/10.1039/C3FD00042G.

Schlesinger, R.B., 2007. The health impact of common inorganic components of fine particulate matter (PM2.5) in ambient air: a critical review. Inhal. Toxicol. 19, 811–832. https://doi.org/10.1080/08958370701402382.

Shalamzari, M.S., Kahnt, A., Vermeylen, R., Kleindienst, T.E., Lewandowski, M., Cuyckens, F., Maenhaut, W., Claeys, M., 2014. Characterization of polar organosulfates in secondary organic aerosol from the green leaf volatile 3-Z-hexenal. Environ. Sci. Technol. 48, 12671–12678. https://doi.org/10.1021/es503226b.

Sheesley, R.J., Schauer, J.J., Bean, E., Kenski, D., 2004. Trends in secondary organic aerosol at a remote site in Michigan's upper peninsula. Environ. Sci. Technol. 38, 6491–6500. https://doi.org/10.1021/es049104q.

Singh, N., Murari, V., Kumar, M., Barman, S.C., Banerjee, T., 2017. Fine particulates over South Asia: review and meta-analysis of PM2.5 source apportionment through receptor model. Environ. Pollut. 223, 121–136. https://doi.org/10.1016/j.envpol.2016.12.071.

Slade, Jonathan H., Ault, Andrew P., Bui, Alexander T., Ditto, Jenna C., Lei, Ziying, Bondy, Amy L., Olson, Nicole E., Cook, Ryan D., Desrochers, Sarah J., Harvey, Rebecca M., Erickson, Matthew H., Wallace, Henry W, Alvarez, Sergio L., Flynn, James H., Boor, Brandon E., Petrucci, Giuseppe A., Gentner, Drew R., Griffin, Robert J., Shepson, Paul B., 2019. Bouncier Particles at Night: Biogenic Secondary Organic Aerosol Chemistry and Sulfate Drive Diel Variations in the Aerosol Phase in a Mixed Forest. Environmental Science & Technology 53 (9), 4977–4987. https://doi.org/10.1021/acs.est.8b07319.

Spak, S.N., Holloway, T., 2009. Seasonality of speciated aerosol transport over the Great Lakes region. J. Geophys. Res. Atmos. 114 https://doi.org/10.1029/2008jd010598.

Spicer, C.W., 1977. Photochemical atmospheric pollutants derived from nitrogen oxides. Atmos. Environ. 11, 1089–1095. https://doi.org/10.1016/0004-6981(77)90239-6, 1967.

Stein, A.F., Draxler, R.R., Rolph, G.D., Stunder, B.J.B., Cohen, M.D., Ngan, F., 2015. NOAA's HYSPLIT atmospheric transport and dispersion modeling system. Bull. Am. Meteorol. Soc. 96, 2059–2077. https://doi.org/10.1175/bams-d-14-00110.1.

Stelson, A.W., Seinfeld, J.H., 1982. Thermodynamic prediction of the water activity, NH4NO3 dissociation constant, density and refractive index for the NH4NO3-(NH4) 2SO4-H2O system at 25°C. Atmos. Environ. 16, 2507–2514. https://doi.org/10.1016/0004-6981(82)90142-1, 1967.

Stone, E.A., Hedman, C.J., Sheesley, R.J., Shafer, M.M., Schauer, J.J., 2009. Investigating the chemical nature of humic-like substances (HULIS) in North American atmospheric aerosols by liquid chromatography tandem mass spectrometry. Atmos. Environ. 43, 4205–4213. https://doi.org/10.1016/j.atmosenv.2009.05.030.

Surratt, J.D., Chan, A.W.H., Eddingsaas, N.C., Chan, M., Loza, C.L., Kwan, A.J., Hersey, S. P., Flagan, R.C., Wennberg, P.O., Seinfeld, J.H., 2010. Reactive intermediates revealed in secondary organic aerosol formation from isoprene. Proc. Natl. Acad. Sci. U.S.A. 107, 6640–6645. https://doi.org/10.1073/pnas.0911114107.

Surratt, J.D., Gómez-González, Y., Chan, A.W.H., Vermeylen, R., Shahgholi, M., Kleindienst, T.E., Edney, E.O., Offenberg, J.H., Lewandowski, M., Jaoui, M., Maenhaut, W., Claeys, M., Flagan, R.C., Seinfeld, J.H., 2008. organosulfate formation in biogenic secondary organic aerosol. J. Phys. Chem. A. 112, 8345–8378. https://doi.org/10.1021/jp802310p.

Surratt, J.D., Lewandowski, M., Offenberg, J.H., Jaoui, M., Kleindienst, T.E., Edney, E.O., Seinfeld, J.H., 2007. Effect of acidity on secondary organic aerosol formation from isoprene. Environ. Sci. Technol. 41, 5363–5369. https://doi.org/10.1021/es0704176.

Tolocka, M.P., Turpin, B., 2012. Contribution of organosulfur compounds to organic aerosol mass. Environ. Sci. Technol. 46, 7978–7983. https://doi.org/10.1021/es300651v.

Valavanidis, A., Fiotakis, K., Vlachogianni, T., 2008. Airborne particulate matter and human health: toxicological assessment and importance of size and composition of particles for oxidative damage and carcinogenic mechanisms. J. Environ. Sci. Health, Part C 26, 339–362. https://doi.org/10.1080/10590500802494538.

Vermeuel, M.P., Novak, G.A., Alwe, H.D., Hughes, D.D., Kaleel, R., Dickens, A.F., Kenski, D., Czarnetzki, A., Stone, E.A., Stanier, C.O., Pierce, R.B., Millet, D.B., Bertram, T.H., 2019. Sensitivity of ozone production to NOx and VOC along the lake Michigan coastline. J. Geophys. Res. Atmos. https://doi.org/10.1029/2019jd030842, 0.

Wang, J., Ogawa, S., 2015. Effects of meteorological conditions on PM2.5 concentrations in Nagasaki, Japan. Int. J. Environ. Res. Publ. Health 12, 9089–9101. https://doi.org/10.3390/ijerph120809089.

Wang, Y., Hu, M., Guo, S., Wang, Y., Zheng, J., Yang, Y., Zhu, W., Tang, R., Li, X., Liu, Y., 2018. The secondary formation of organosulfates under interactions between biogenic emissions and anthropogenic pollutants in summer in Beijing. Atmos. Chem. Phys. 18, 10693–10713. https://doi.org/10.5194/acp-18-10693-2018.

Whiteaker, J.R., Suess, D.T., Prather, K.A., 2002. Effects of meteorological conditions on aerosol composition and mixing state in Bakersfield, CA. Environ. Sci. Technol. 36, 2345–2353. https://doi.org/10.1021/es011381z.

Zhang, H., Surratt, J.D., Lin, Y.H., Bapat, J., Kamens, R.M., 2011. Effect of relative humidity on SOA formation from isoprene/NO photooxidation: enhancement of 2-methylglyceric acid and its corresponding oligoesters under dry conditions. Atmos. Chem. Phys. 11, 6411–6424. https://doi.org/10.5194/acp-11-6411-2011.

Zhang, H., Worton, D.R., Lewandowski, M., Ortega, J., Rubitschun, C.L., Park, J.-H., Kristensen, K., Campuzano-Jost, P., Day, D.A., Jimenez, J.L., Jaoui, M., Offenberg, J. H., Kleindienst, T.E., Gilman, J., Kuster, W.C., De Gouw, J., Park, C., Schade, G.W., Frossard, A.A., Russell, L., Kaser, L., Jud, W., Hansel, A., Cappellin, L., Karl, T., Glasius, M., Guenther, A., Goldstein, A.H., Seinfeld, J.H., Gold, A., Kamens, R.M., Surratt, J.D., 2012. Organosulfates as tracers for secondary organic aerosol (SOA) formation from 2-Methyl-3-Buten-2-ol (MBO) in the atmosphere. Environ. Sci. Technol. 46, 9437–9446. https://doi.org/10.1021/es301648z.

Zhang, Y., Huang, J.-P., Henze, D.K., Seinfeld, J.H., 2007. Role of isoprene in secondary organic aerosol formation on a regional scale. J. Geophys. Res. Atmos. 112 https://doi.org/10.1029/2007jd008675.